

TKK Dissertations 194
Espoo 2009

**DESIGN AND CHARACTERIZATION OF
SINGLE-PHASE POWER FILTERS**

Doctoral Dissertation

Konstantin Kostov



**Helsinki University of Technology
Faculty of Electronics, Communications and Automation
Department of Electrical Engineering**

TKK Dissertations 194
Espoo 2009

DESIGN AND CHARACTERIZATION OF SINGLE-PHASE POWER FILTERS

Doctoral Dissertation

Konstantin Kostov

Dissertation for the degree of Doctor of Science in Technology to be presented with due permission of the Faculty of Electronics, Communications and Automation for public examination and debate in Auditorium S4 at Helsinki University of Technology (Espoo, Finland) on the 27th of November, 2009, at 12 noon.

**Helsinki University of Technology
Faculty of Electronics, Communications and Automation
Department of Electrical Engineering**

**Teknillinen korkeakoulu
Elektroniikan, tietoliikenteen ja automaation tiedekunta
Sähkötekniikan laitos**

Distribution:

Helsinki University of Technology
Faculty of Electronics, Communications and Automation
Department of Electrical Engineering
P.O. Box 3000 (Otakaari 5)
FI - 02015 TKK
FINLAND
URL: <http://sahkotekniikka.tkk.fi/en/>
Tel. +358-9-47001
E-mail: konstantin.kostov@tkk.fi

© 2009 Konstantin Kostov

ISBN 978-952-248-186-3
ISBN 978-952-248-187-0 (PDF)
ISSN 1795-2239
ISSN 1795-4584 (PDF)
URL: <http://lib.tkk.fi/Diss/2009/isbn9789522481870/>

TKK-DISS-2669

Picaset Oy
Helsinki 2009



ABSTRACT OF DOCTORAL DISSERTATION		HELSINKI UNIVERSITY OF TECHNOLOGY P.O. BOX 1000, FI-02015 TKK http://www.tkk.fi	
Author Konstantin Kostov			
Name of the dissertation Design and Characterization of Single-Phase Power Filters			
Manuscript submitted 15.05.2009		Manuscript revised 02.10.2009	
Date of the defence 27.11.2009			
<input type="checkbox"/> Monograph		<input checked="" type="checkbox"/> Article dissertation (summary + original articles)	
Faculty Electronics, Communications and Automation			
Department Electrical Engineering			
Field of research Industrial Electronics and Electric Drives			
Opponent(s) Prof. Johann W. Kolar			
Supervisor Prof. Jorma Kyyrä			
Instructor			
Abstract <p>In order to comply with the strict limits on electromagnetic emissions from electrical and electronic equipment, most switch-mode power supplies need an <i>electromagnetic interference</i> (EMI) filter at their input. This dissertation discusses issues related to the design of passive single-phase power filters, such as noise sources, coupling paths, parasitic elements, and suggests analytical tools to simplify and improve the design. The most important recommendations and steps in the design of single-phase power filters are outlined. The starting point in any design procedure is to determine the required <i>insertion loss</i> (IL), which depends on the <i>common-mode</i> (CM) and <i>differential-mode</i> (DM) noise generated by the electrical equipment. This requires the use of noise separators, which split the EMI generated by the equipment under test into its CM and DM components. The advantages and disadvantages of different noise separation techniques are discussed and some of them are shown to be inaccurate. Even when an appropriate noise separator is used, it is necessary to know what kind of data are obtained, because there are different definitions for CM and DM. Misinterpreted or inaccurate data for the CM and DM noise lead to wrong attenuation requirements, the consequence of which is either overdesign, or worse, failure to suppress the noise sufficiently.</p> <p>A major obstacle for predicting the performance of EMI filters are the unknown noise source impedances. Methods for noise source impedance measurement have been suggested in the literature and are discussed in the thesis. These methods are difficult, time-consuming, and some of them incorrect.</p> <p>Traditionally, EMI suppression filters and components are characterized by their IL. In this work two- and four-port network parameters are used to obtain the IL or equivalent circuits of the filter. It is suggested that the “worst-case” IL can be obtained from the chain parameters of the filter or component. Although the concept of IL applies to two-port networks, equations for the CM and DM IL of four-port networks as functions of their four-port network parameters and arbitrary source and load impedances are derived and verified. The four-port network parameters can also be used to obtain the elements of the CM and DM π-type equivalent circuits of a single-phase EMI filter. A new way to define the CM and DM suppression requirements as a part of the total required IL is proposed in the thesis.</p>			
Keywords Electromagnetic compatibility, insertion loss, passive filters, power filters, scattering parameters			
ISBN (printed) 978-952-248-186-3		ISSN (printed) 1795-2239	
ISBN (pdf) 978-952-248-187-0		ISSN (pdf) 1795-4584	
Language English		Number of pages 80 + 56	
Publisher Helsinki University of Technology, Department of Electrical Engineering			
Print distribution Helsinki University of Technology, Department of Electrical Engineering			
<input checked="" type="checkbox"/> The dissertation can be read at http://lib.tkk.fi/Diss/2009/isbn9789522481870/			

Preface

This dissertation is a result of my work in the Laboratory of Power Electronics, currently Department of Electrical Engineering, at the Helsinki University of Technology. I have been working there since 2001 as a teaching or research assistant, and later as a researcher. I had the chance to work in different projects with different colleagues and students, but I was always under the supervision of Prof. Jorma Kyyrä, who was recently appointed vice-rector of Aalto University. No doubt this is good for the new University, but our department loses a great expert, teacher and manager. I am deeply grateful to Prof. Kyyrä for all he did for me and wish him well in his new position.

Next, I would like to thank the colleagues who coauthored some of the publications in this thesis. In the beginning of my research career I had the privilege to work with Prof. Teuvo Suntio. The fact that we are coauthors in eleven publications is an indication of how much I benefited from his deep knowledge of power supplies. I also had the pleasure to share an office with D.Sc. Vesa Tuomainen for several years. Our discussions covered a wide variety of topics, from politics to power electronics, but I must mention his help in troubleshooting my first prototype. The other two of my coauthors, M.Sc. Jukka-Pekka Sjöroos and Antti Niinikoski, are also my ex-colleagues. Thank you all for your help and cooperation!

All my colleagues, past and present, in the Department of Electrical Engineering deserve thanks for their work and support. Despite the challenges, inevitable in any work place, I enjoyed my eight years in the department and see many of you as friends. I say to all that shared office with me, worked in the lab, or just visited the cafeteria: Thank you for your friendship, company, advice, or encouragement!

It is hard to overestimate the role of money in this world, and the academic work is no exception. In this regard I owe gratitude to several companies and organizations, which supported my work. In the beginning, a major part of my funding came from TEKES, the Finnish Funding Agency for Technology and Innovation; Nokia Networks Oy; PKC Group Oy; and Salkomp Oy. From 2004 until the end of 2007 my research was funded mainly by the Graduate School of Electrical Engineering. In 2008 and 2009 part of my funding came from TKK/MIDE through its HybLab project. I appreciate also the financial grants from the Research Foundation of Helsinki University of Technology and from Nokia Foundation.

I cannot end this preface without mentioning my family. My wife Tiina and our boys, Patrick and Samuel, give joy and meaning to my life. I appreciate their love, support, and sacrifice. My greatest wish is to balance work and family life better and be more present in their lives.

Espoo, October 2009
Konstantin Kostov

Contents

Preface	5
Contents	7
List of Publications	9
List of Abbreviations	11
List of Symbols	13
List of Figures	15
1 Introduction	17
1.1 Background and Scope	17
1.2 Summary of Publications	18
1.3 Scientific Contribution	20
1.4 Structure of the Thesis.....	21
2 Conducted Electromagnetic Emissions	23
2.1 Classification of Electromagnetic Emissions	23
2.2 Measurement of Conducted Emissions	23
2.3 CM and DM Conducted Emissions	26
2.4 Conducted Noise Separation	29
2.5 Noise Source Impedance	34
3 Passive Power Filters	37
3.1 Topology.....	37
3.2 Equivalent Circuits	38
3.3 Components	39
3.3.1 Resistors	40
3.3.2 Capacitors.....	40
3.3.3 Inductors.....	42
4 Characterization and Design of Power Filters	47
4.1 Insertion Loss	47
4.1.1 Insertion Loss in Terms of Two-Port Parameters	48
4.1.2 Insertion Loss in Terms of Four-Port Parameters	49
4.2 CM and DM Π -equivalent Circuits	52
4.3 EMI Filter Design.....	53
4.3.1 Determine the CM and DM Suppression Requirements.....	53
4.3.2 Selecting Filter Topology.....	55
4.3.3 Selecting Filter Components	55
4.3.4 Layout Design	56
4.3.5 Check Performance of the SMPS with Filter	57
5 Conclusions	59
References	61
Appendices	65
A.1 Network Parameters	67

A.1.1	N-Port Network Parameters	67
A.1.2	Two-Port Network Parameters.....	69
A.2	The Input Impedances of Some Noise Separators.....	73
A.2.1	The Resistive Noise Separator in Figure 2.8a.....	73
A.2.2	The Transformer-Based Noise Separators in Figure 2.9a and c	73
A.3	Symmetrical T- and Π -Equivalents of the Diagonal Circuit.....	75
A.3.1	The Diagonal Circuit.....	75
A.3.2	The T-circuit.....	76
A.3.3	Symmetrical T-equivalent of the Symmetrical Diagonal Circuit	76
A.3.4	The Π -circuit	77
A.3.5	Symmetrical Π -equivalent of the Symmetrical Diagonal Circuit	78
A.4	CM and DM Inductance of Coupled Inductors	79

List of Publications

This thesis consists of an overview and the following publications which are referred to in the text by their Roman numerals:

- I Konstantin Kostov, J. Kyyrä, and T. Suntio: *Analysis and Design of EMI Filters for DC-DC Converters Using Chain Parameters*, EPE 2003, Toulouse, France, September 2003, p. 10.
- II Konstantin Kostov, J.-P. Sjöroos, J. Kyyrä, and T. Suntio: *Selection of Power Filters for Switched Mode Power Supplies*, NORPIE 2004, Trondheim, Norway, June 2004, p. 7.
- III Konstantin Kostov, A. Niinikoski, J. Kyyrä, and T. Suntio: *Prediction of the Conducted EMI from DC-DC Switched-Mode Power Converters*, EPE-PEMC 2004, Riga, Latvia, September 2004, p. 5.
- IV Konstantin Kostov, V. Tuomainen, J. Kyyrä, and T. Suntio: *Designing Power Line Filters for DC-DC Converters*, EPE-PEMC 2004, Riga, Latvia, September 2004, p. 6.
- V Konstantin Kostov and J. Kyyrä: *Insertion Loss and Network Parameters in the Analysis of Power Filters*, NORPIE 2008, Espoo, Finland, June 2008, p. 5.
- VI Konstantin Kostov and J. Kyyrä: *Insertion Loss in Terms of Four-Port Network Parameters*, IET Science, Measurement and Technology, Vol. 3, Iss. 3, May 2009, pp. 208-216.
- VII Konstantin Kostov and J. Kyyrä: *Common-Mode Choke Coils Characterization*, EPE 2009, Barcelona, Spain, September 2009, p. 9.

The author wrote the above publications under the supervision of Prof. Jorma Kyyrä. Discussions with and advice from Prof. Teuvo Suntio helped in the preparation of Publications I – IV. Jukka-Pekka Sjöroos and Antti Niinikoski helped with the measurements in Publications II and III, respectively. Dr. Vesa Tuomainen helped in the preparation of the prototypes for Publication IV.

List of Abbreviations

AC	alternating current
AMN	artificial mains network
AV	average (detector)
CISPR	Comité International Spécial des Perturbations Radioélectriques (International Special Committee on Radio Interference)
CM	common-mode
CMRR	common-mode rejection ratio
CMTR	common-mode transmission ratio
DC	direct current
DM	differential-mode
DMRN	DM rejection network
DMRR	DM rejection ratio
DMTR	DM transmission ratio
DPDT	double pole - double throw (switch)
EMC	electromagnetic compatibility
EME	electromagnetic emissions
EMI	electromagnetic interference
EPC	equivalent parallel capacitance
EPR	equivalent parallel resistance
ESL	equivalent series inductance
ESR	equivalent series resistance
EU	European Union
EUT	equipment under test
HF	high-frequency
IEC	International Electrotechnical Commission
IL	insertion loss
LISN	line impedance stabilization network
PCB	printed circuit board
QP	quasi-peak (detector)
RF	radiofrequency
SMPC	switched-mode power converter
SMPS	switched-mode power supply
SRF	self-resonant frequency
VNA	vector network analyzer

List of Symbols

In general, quantities denoted with small italic letters refer to instantaneous values and capital italic letters refer to *root-mean square* (rms) values. Capital and small letters in bold refer to matrices and vectors, respectively. When a subscript in a symbol corresponds to an abbreviation from the list of abbreviations, then the symbol refers to the abbreviated quantity or parameter, e.g. I_{cm} would refer to the rms value of the CM current.

$ $	impedances connected in parallel
C	capacitance, F
C_c	cancellation capacitance, F
C_p	parasitic capacitance, F
C_X	X-capacitor, F
C_Y	Y-capacitor, F
i	instantaneous current, A
i_c	instantaneous current through a capacitance, A
i_g, I_g	instantaneous and rms value of the ground current, A
IL	insertion loss, dB
IL'	insertion loss with $Z_s = Z_L = Z_0$, dB
$IL_{cm,req}$	required CM insertion loss, dB
$IL_{dm,req}$	required DM insertion loss, dB
i_p, i_n	phase and neutral instantaneous currents, A
I_p, I_n	rms of the phase and neutral currents, A
IR	insertion ratio
$J_{s,dm}$	DM noise current source, A
k	coupling coefficient
L	inductance, H
n	turns ratio
P_2, P_{20}	active power delivered to the load with and without filter inserted between it and the generator, W
R	resistance, Ω
R_0	resistive reference impedance, usually 50 Ω
v	instantaneous voltage, V
V	rms voltage, V
v_c	instantaneous voltage across a capacitance, V
$V_{cm,m}$	rms of the measured CM voltage, V
$V_{dm,m}$	rms of the measured DM voltage, V

v_p, v_n	phase or neutral instantaneous voltages, V
V_p, V_n	rms of the phase and neutral voltages, V
$V_{p/n,max}$	maximum noise voltage at the phase or neutral, V
$V_{s,cm}, V_{s,dm}$	rms of the CM and DM noise source voltages, V
Y	admittance, S
Y_c	admittance of a capacitor, S
Y_{ind}	admittance of an inductor, S
Z	impedance, Ω
Z_0	reference impedance, Ω
Z_b	input “bulk” capacitor impedance, Ω
Z_c	impedance of a capacitor, Ω
Z_i	impedance seen from the i^{th} port of an n -port network, Ω
$Z_{i,cp}$	insertion impedance of a current probe, Ω
$Z_{i,in}$	input impedance at the i^{th} port of an n -port network, Ω
$Z_{in,c}$	input impedance of a power converter, Ω
$Z_{in,n}$	noise separator’s neutral port input impedance, Ω
$Z_{in,p}$	noise separator’s phase port input impedance, Ω
Z_L	load impedance, Ω
Z_m	input impedance of a measurement instrument, Ω
Z_n	power line’s neutral-to-ground impedance, Ω
Z_p	power line’s phase-to-ground impedance, Ω
Z_s	source impedance, Ω
$Z_{s,cm}$	CM noise source impedance, Ω
$Z_{s,dm}$	DM noise source impedance, Ω
$Z_{s,n}$	neutral-to-ground noise source impedance, Ω
$Z_{s,p}$	phase-to-ground noise source impedance, Ω
ρ_L	load reflection coefficient
ρ_s	source reflection coefficient

List of Figures

Figure 2.1: An example of a measurement setup for conducted emissions test.	24
Figure 2.2: Conducted emissions measurement circuit.	24
Figure 2.3: The output impedance of a $50\ \Omega / 50\ \mu\text{H}$ LISN.	25
Figure 2.4: Conducted noise limits.	26
Figure 2.5: HF equivalent of the conducted emissions measurement circuit.	27
Figure 2.6: Another HF equivalent of the conducted emissions measurement circuit. .	28
Figure 2.7: Measuring CM or DM noise with a current probe.	30
Figure 2.8: Examples of different types of noise separators:	33
Figure 2.9: Wideband transformer-based noise separator designs:	34
Figure 3.1: A two-stage passive power filter with its equivalent circuits:	38
Figure 3.2: Capacitor's equivalent circuits and parasitics cancellation:	41
Figure 3.3: Equivalent circuits for two-terminal inductor:	42
Figure 3.4: EPC cancellation for decoupled DM inductors:	43
Figure 3.5: EPC cancellation for CM chokes:	44
Figure 3.6: EPC cancellation for coupled DM inductors:	44
Figure 4.1: Insertion loss definition:	47
Figure 4.2: Measurement test circuits:	50
Figure 4.3: <i>a)</i> A general two-port network; <i>b)</i> π -equivalent circuit.	52
Figure A.1: An n -port network.	67
Figure A.2: A two-port network.	69
Figure A.3: Electrical circuit of the resistive noise separator in Figure 2.8 <i>a</i>	73
Figure A.4: Equivalent circuit of the noise separators in Figure 2.9 <i>a</i> and <i>c</i>	74
Figure A.5: The diagonal circuit:	75
Figure A.6: T-equivalent of a symmetrical diagonal circuit:	76
Figure A.7: Π -equivalent of a symmetrical diagonal circuit:	77
Figure A.8: <i>a)</i> CM choke; <i>b)</i> coupled DM inductors.	79

1 Introduction

1.1 Background and Scope

Most of the electrical energy distribution takes place through the AC power lines, but an increasing number of loads consume DC energy. The primary technology for converting AC and DC energy into energy suitable for DC loads is *switched-mode power supplies* (SMPSs). Often, the only difference between AC-DC and DC-DC SMPSs is that the latter do not have a rectifier at their input. The essential point in all *switched-mode power converters* (SMPCs), including AC-AC converters, is that they rapidly switch one or more power transistors between saturation, i.e. fully on-state, and fully off-state, with a variable duty cycle, and possibly a variable frequency. The result of this switching is an almost rectangular voltage and/or current waveforms, which, depending on the requirements of the load, may be filtered to achieve the desired output.

The main advantage of the switched-mode power conversion is greater efficiency, because the switching transistor dissipates much less energy in saturated and off-state compared to its semiconducting state. Higher efficiency also means less heat produced by a SMPC with a given rating. Other advantages are the smaller size and weight as a result of the elimination of low-frequency transformers, but also because at higher switching frequencies the ripple requirements can be fulfilled with smaller inductors and capacitors.

Unfortunately, the gains in efficiency, size, and weight do not come for free. SMPSs have greater complexity and generate a large amount of *electromagnetic emissions* (EME), which can disturb the operation of an electrical or electronic device itself or other equipment in its environment.

Concern about the *electromagnetic interference* (EMI) caused by EME started long before the arrival of SMPS. At its Paris meeting in 1933 [1], the *International Electrotechnical Commission* (IEC) recommended the formation of the *International Special Committee on Radio Interference* (CISPR, from *Comité International Spécial des Perturbations Radioélectriques* in French) to deal with the problems caused by increasing electromagnetic pollution. Over the years there has been substantial growth not only in the amount of electronic equipment, but also in its complexity, which makes modern systems more susceptible to various types of EMI. These tendencies lead to a narrowing “compatibility gap” [2], which can be maintained by limiting the EME on one hand, and requiring a certain level of immunity on the other. This is the purpose of the CISPR standards, which specify the emissions and susceptibility limits, their methods of measurement, the equipment used, etc. In most cases, including the *European Union* (EU), the CISPR standards have been adopted by governments and used as legal requirements for all products sold on the market.

Compliance with the strict regulations and safety requirements has forced the industry to pay serious attention to *electromagnetic compatibility* (EMC) issues. From technical

point of view, the problems in dealing with these issues arise from the difficulty of identifying the sources and coupling paths through which the noise propagates and affects the victim. If these were known, their modeling and analysis would lead to effective solutions. Instead, many practicing engineers consider EMC a kind of “black magic” [3]-[4].

This dissertation deals with single-phase passive power filters, which are used for conducted noise suppression. Active power filters can also be used for the same purpose, but, as they operate in a fundamentally different way, they are outside the scope of the thesis. So far, passive power filters have been the most popular remedy for conducted EME because of their reliability, simplicity, and effectiveness.

The noise attenuation requirements can be eased by applying various techniques for noise suppression at source. These techniques must not be overlooked, but in most cases, despite all the efforts, input or EMI filters, as they are also called, are necessary to meet the emissions limits. Arguably, compliance with the regulations for conducted emissions is a prerequisite for meeting the radiated EME limits. The reason is that conductors can be viewed as antennas and if the limits on conducted noise are not met, it is unlikely that the limits for radiated emissions will be fulfilled.

The objective of this work is to explore the issues involved in the design of passive power filters and suggest some analytical tools that can simplify and improve power filter design. It discusses the noise sources, coupling paths, and parasitic elements, which affect EMI filter design. The advantages and disadvantages of different noise separation techniques are considered and the use of network parameters in the modeling, analysis, and design of passive power filters and components is presented.

1.2 Summary of Publications

Publication I

This paper demonstrates how chain parameters can be used to calculate the *insertion loss* (IL) of an EMI filter and in the input system stability analysis. The stability analysis shows that even very small resistances in series with the capacitor and inductor, closest to the input of the SMPC, can compensate the effect of converter’s negative input impedance.

A comparison between LC- and π -filter shows that if the impedance of the power line is very low, an LC-filter will perform just as a π -filter. However, when the source impedance is high or unknown it is recommended to use π -filter.

Publication II

Power filter manufacturers provide IL measurement data for their products. In most cases these data are measured with $50\ \Omega$ source and load impedance. In some cases the so-called “approximate worst case measurements” are published as well. The goal of this publication was to find out which of these data should be considered when selecting an off the shelf input filter for a SMPS. The results show that, the actual *common-mode*

(CM) attenuation of a filter operating with a buck converter is almost same as the published IL data with $0.1 \Omega/100 \Omega$ source/load impedances, whereas the actual *differential-mode* (DM) IL is closer to the published IL data with reversed source and load impedances, i.e. the $100 \Omega/0.1 \Omega$ data.

Publication III

This paper presents theoretical estimation of the conducted EME from a SMPS, based on Fourier analysis. The theory is applied to a buck converter. The comparison between the theoretically estimated and measured EMI shows that the CM EMI was well predicted. Up to 3 MHz the measured DM noise was much lower than the predicted one, which could be because of the unknown DM noise source impedance.

Publication IV

A method for designing power line filters for SMPS is presented, which reduces the trial-and-error design work, by excluding the nonviable combinations of filter components. The designer can choose among the theoretically viable combinations, to try practical designs. The theoretical calculations are based on chain parameters. As an illustration of the method a single stage π -filter for a buck converter is designed. The results prove the design procedure to be simple and straightforward.

Publication V

This paper discusses the IL definitions and suggests as an alternative to use network parameters. It is a known fact that the standard IL measurements do not provide reliable information about the operational performance of a suppressor. This is largely due to the source and load mismatch, which is typical in power lines. Arguments are presented, showing that network parameters allow for more complete and reliable characterization of power filters and components. The IL does not have to be abandoned, because the network parameters provide enough information to obtain not only the standard IL, but also the IL in a non 50Ω system. A new treatment of “worst case” or minimum IL is proposed, which is also based on network parameters. Furthermore, input, output, or transfer impedances, simulation models, and other characteristics, can be obtained from the network parameters, but not from the currently published standard IL data.

Publication VI

By definition, the IL is applicable to two-port networks, but most filters have a higher number of ports. Single-phase power filters are four-port networks and measurements of their suppression characteristics require one measurement for the CM and another for the DM IL. Normally, the measurement apparatus have unbalanced ports and CM measurements are relatively easy to perform. However, the DM measurements require balanced–unbalanced conversion at the input and output of the filter. Wideband transformers (baluns) are used for this conversion. Instead of measuring it directly, the CM or DM IL can be calculated from the four-port parameters of the filter. The equations for IL in terms of four-port network parameters are derived theoretically and verified exper-

rimentally. The adoption of four-port parameters in engineering practice would reduce the amount of measurement work and increase the reliability and repeatability of the results because the use of baluns or other changes in the *equipment under test* (EUT) are not necessary.

Publication VII

This paper reviews the models for two- and four-terminal inductors and presents two methods to obtain the CM and DM characteristics of four-terminal devices, like CM chokes. More specifically, it shows how the IL and π -equivalent circuits of a CM choke can be obtained using two- and four-port network parameters. However, these characterization methods are applicable not only to CM chokes, but to any four-terminal component or network, such as single-phase power filters.

The measurements show that second order linear circuit models cannot describe accurately the CM and DM characteristics of a CM choke over a wide frequency range. For the studied example, the DM characteristics were more complex than the CM ones.

1.3 Scientific Contribution

The most important scientific contributions of this thesis can be summarized as follows:

- In Section 2.3 two different definitions for DM and CM found in the literature are pointed out. These differences can lead to misinterpretation of the conducted noise measurement data and setting wrong attenuation requirements for the design. The result is either overdesign or failure to suppress the EME sufficiently.
- A noise source model is suggested in Figure 2.6 suitable for single-phase systems. The noise source impedances are usually unknown, which is a major obstacle in the analysis of EMI filters. Section 2.4 discusses the noise source impedance measurement methods suggested in the literature. Only two of them were found to be theoretically accurate, but they are time-consuming and difficult to implement.
- The use of network parameters in the analysis and modeling of power filters is demonstrated in Chapter 4 and in most of the Publications. Details on the use of chain parameters can be seen in Publications I-II, IV-V and VII, on z -parameters in Publications V-VI, more on y -parameters in Publication VI, and on s -parameters in Publications V-VII.
- A new way to determine the suppression requirements is given in sub-section 4.3.1. The required CM and DM noise attenuation can be specified in proportion of the required total attenuation.
- Section 4.3 presents the most essential steps in the design of single-phase power filters. The design procedure proposed in Publication IV is for DC-DC power filters, but it can be applied to single-phase ac filters as well.
- In Publication V it is suggested that the “worst-case” IL of a filter can be obtained from its chain parameters.

- Sub-section 4.1.2 presents the equations for IL in terms of four-port network parameters and arbitrary source and load impedances. The derivation and verification of these equations are in Publication VI.
- Any single-phase EMI filter, regardless of its topology and number of stages, can be replaced by two π -type equivalent circuits, one for CM and another for DM. Section 4.2 and Publication VII show how the elements of these equivalent circuits can be obtained from the network parameters of the filter.

1.4 Structure of the Thesis

This dissertation is organized as follows:

- Chapter 1 defines the scope of the thesis and its contributions and structure.
- Chapter 2 gives a short overview of EME, their limits, measurement, auxiliary equipment, and factors affecting the propagation of conducted EME. Originally this material was intended to provide the necessary background for the design and characterization of power filters. However, it also points out the inconsistent CM and DM definitions in the literature; it warns against and endorses certain methods for noise separation and noise source impedance measurement.
- Chapter 3 reviews the topologies, equivalent circuits, and the components of passive single-phase power filters. The use of symmetrical topologies is recommended and methods for cancelling the parasitics of capacitors and inductors are briefly reviewed.
- Chapter 4 focuses on the characterization of power filters. Traditionally, the IL has been used to characterize suppression filters or components, but it has limitations, many of which can be overcome by using network parameters. The last section of Chapter 4 outlines the most important steps in the design of EMI filters. Depending on the application there can be variations or additional design steps, which can be found in the suggested references.
- Chapter 5 summarizes the conclusions and suggests topics for future research.
- The Appendices contain definitions of network parameters, derivation of the input impedances of some noise separators, derivation of the π - and T-equivalents of symmetrical diagonal circuits, and derivation of the CM and DM inductances of coupled inductors.

The publications included in this dissertation are reprinted at the end.

2 Conducted Electromagnetic Emissions

2.1 Classification of Electromagnetic Emissions

Depending on the propagation medium, EME can be divided into radiated and conducted emissions. Radiated emissions propagate through space and conducted emissions propagate through interface and power cables. It may appear that CISPR makes this division on the basis of frequency, because it limits the conducted emissions from 150 kHz to 30 MHz and the radiated emissions from 30 MHz to 1 GHz, but this does not mean that there are no radiated emissions below 30 MHz or conducted emissions above 30 MHz. The reason for this frequency separation is that below/above 30 MHz the radiated/conducted emissions are not dominant.

According to their origin, radiated emissions can be divided into radiated from the *printed circuit boards* (PCBs) and from cables [2]. The main remedy for radiated EMI is shielding, but before this is used, efforts should be made to achieve a good PCB layout and grounding. The radiated emissions originating from cables can be reduced most effectively by suppressing the conducted emissions propagating through them. Therefore, the suppression of conducted emissions, which is the objective of the EMI filters discussed in this thesis, has an impact on radiated emissions as well.

When compared to a reference bandwidth, EME can be classified as narrowband and broadband [2]-[3]. Without going into the details, the frequency spectrum of a broadband electromagnetic disturbance is continuous and covers a relatively wide range. Broadband conducted disturbances can be caused by random switching events, digital data transfer, re-conducted radiated emissions, and other mostly parasitic phenomena. Provided the electrical equipment has a good layout, grounding, and components, its broadband emissions are unlikely to be a cause for concern. The limits set in the standards are usually exceeded by the narrow peaks in the noise spectrum, i.e. the narrowband emissions. These can be caused by oscillator and signal harmonics, but most often by the SMPS of the equipment.

2.2 Measurement of Conducted Emissions

An example of a measurement setup for conducted emissions tests according to CISPR 16-2-1 [5] is shown in Figure 2.1. Although the physical setup may vary, the conducted emissions test for any electrical equipment supplied by single-phase AC or DC power can be represented by the electrical circuit in Figure 2.2.

The EUT is supplied by the power source through an *artificial mains network* (AMN), which consists of two *line impedance stabilization networks* (LISNs). Therefore, from the power flow point of view, the EUT is the load. However, from the conducted EME

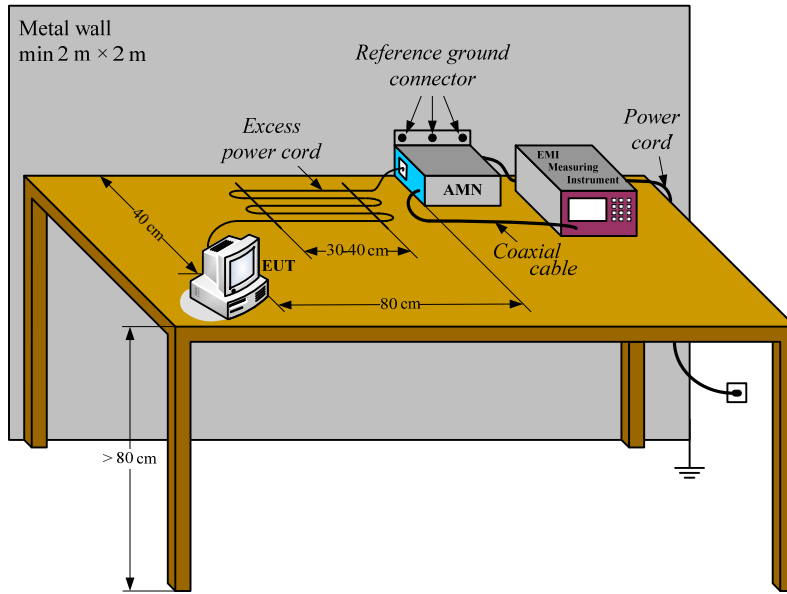


Figure 2.1: An example of a measurement setup for conducted emissions test.

point of view, the EUT is the source because it produces the noise, which should not exceed the limits in the standards. The LISN in the example in Figure 2.2 is known as $50 \Omega / 50 \mu\text{H}$. It provides repeatability of the conducted EMI measurements by fulfilling several important functions:

- It facilitates the power flow from the mains to the EUT. This is done by providing high input-to-ground and low input-to-output impedance for mains frequency and DC signals.
- It prevents *high-frequency* (HF) disturbances from the mains from interfering with the measurements. This function is achieved by providing low input-to-ground and high input-to-output impedance for HF signals.
- It provides well-defined and known output-to-ground impedance for the HF conducted emissions generated by the EUT and guides them to its *radio-frequency* (RF) output.

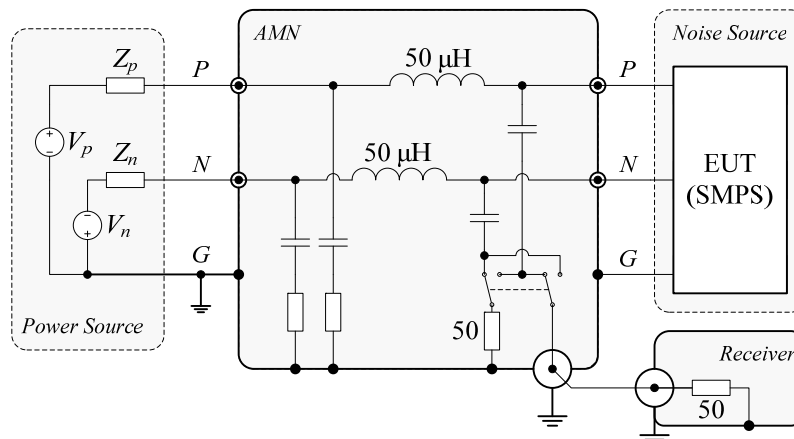


Figure 2.2: Conducted emissions measurement circuit.

The CISPR 16-1-2 standard [6] does not specify the circuit of the LISN, although it suggests one. What is specified in the standard is the output-to-ground impedance of the LISN, as shown in Figure 2.3, which can deviate by $\pm 20\%$ in magnitude. This allows for uncertainty of 20%, which is a lot, but it is much better than the unspecified uncertainty if conducted EMI measurements were performed without AMN. Another advantage of the suggested LISN circuit is that it decouples the impedance seen by the noise from the impedance of the power source very well. This can be evaluated by considering the change of the output impedance of a LISN as a function of the power line impedances, i.e. Z_p and Z_n in Figure 2.2. Increasing the supply line impedance from $0\ \Omega$ to $1\ \text{k}\Omega$ results in a minor increase in the output impedance by only a few ohms below 30-40 kHz. Further increases in the supply line impedance lead to even smaller percentage increases in the output impedance of the LISN. And again, these are only at low frequencies. In the 150 kHz to 30 MHz range the output impedance of the LISN is practically independent of the supply line impedance.

The receiver of the measuring instrument, usually a spectrum analyzer or an EMI test receiver, is connected to the LISN via a coaxial cable. The input impedance of the receiver is $50\ \Omega$, i.e. the same as the output impedance of the LISN. The measuring instrument can be set to use different input bandpass filters or detector functions. These are rigorously defined in CISPR 16-1-1 [7]. In the range 0.15 to 30 MHz, where the conducted noise is most often subject to limitations and must be measured, CISPR requires the use of 9 kHz bandwidth and *average* (AV) or *quasi-peak* (QP) detectors. As its name implies, an AV detector measures the average of the input signal. It has a very long time constant of about 1 s. The specifications for QP detector were established with reference to the human ear [3]. The charging time constant of QP detectors was set to 1 ms, whereas the discharging time constant was set to 160 ms.

CISPR standards, which are usually adopted without change in the EU and most other countries around the world, require the conducted emissions measured from both the

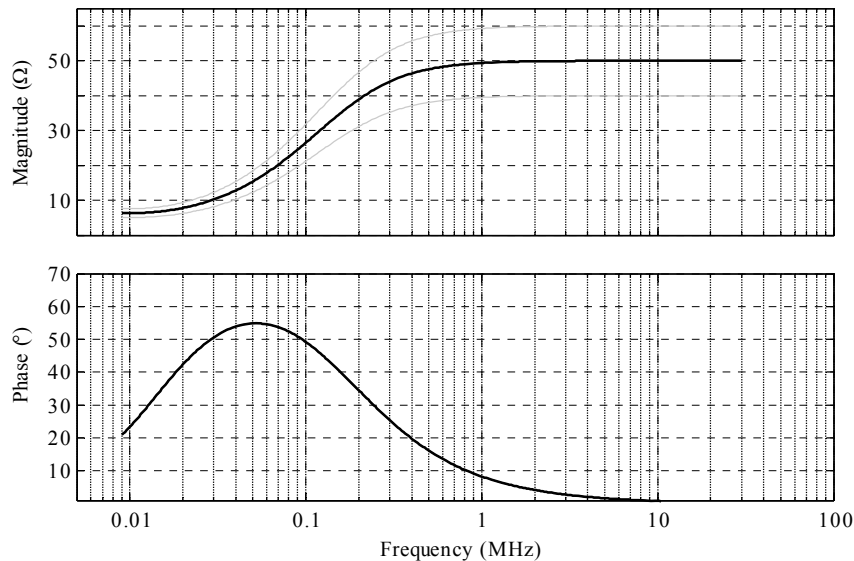


Figure 2.3: The output impedance of a $50\ \Omega / 50\ \mu\text{H}$ LISN.

phase and neutral terminals of a piece of electrical equipment powered by low voltage DC or single-phase AC, with a current rating less than 16 A, not to exceed the limits for its class, as shown in Figure 2.4 for AV and QP detectors [8]-[9]. All products are divided in two classes: Class A for equipment intended for use in industrial environments, and Class B for domestic use.

As with any measurement, the conducted emissions tests are subject to measurement uncertainty that characterizes the expected statistical deviation of the measured values from their true value. There are two types of measurement uncertainties [10]:

- Measurement uncertainties of type A, which are caused by random measurement errors. Such errors, like thermal drift and noise, can be controlled to some extent, but cannot be eliminated or corrected.
- Measurement uncertainties of type B, which are caused by systematic measurement errors. These errors are reproduced repeatedly and can be systematically corrected by calibration. When performing EMC measurements one must be familiar with the measurement instruments in use and their methods of calibration. Full correction of systematic errors is impossible, however, due to superimposed type A errors in the measurements.

The AMN and EMI test receiver used in all conducted EMI measurements presented in Publications II-IV were ESH3-Z5 and ESCS 30 respectively. The *s*-parameters measurements in Publications V-VII were performed with *vector network analyzer* (VNA) ZVL6.

2.3 CM and DM Conducted Emissions

In conducted noise compliance tests the CM and DM noise components are irrelevant. However, they are of the utmost importance in the design and analysis of power filters.

In single-phase applications, the mains cable of the EUT, which is connected to the AMN (Figure 2.2), consists of three parallel wires: phase, neutral, and ground. Some-

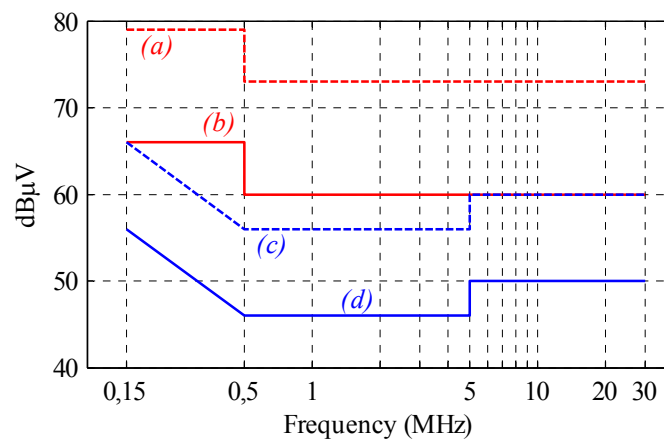


Figure 2.4: Conducted noise limits.

a) Class A, QP detector; *b)* Class A, AV detector; *c)* Class B, QP detector; *d)* Class B, AV detector.

times the power cable might consist of only two wires, only the phase and neutral, in which case the EUT is floating. Let us denote the currents flowing through the phase and neutral conductors with i_p and i_n respectively. According to one school of thought, these currents may be decomposed into two auxiliary currents, which are referred to as the CM current i_{cm} and the DM current i_{dm} :

$$i_p = i_{cm} + i_{dm} \quad i_n = i_{cm} - i_{dm} \quad (2.1)$$

Solving (2.1) for i_{cm} and i_{dm} yields:

$$i_{cm} = \frac{i_p + i_n}{2} \quad i_{dm} = \frac{i_p - i_n}{2} \quad (2.2)$$

The DM currents i_{dm} are equal in magnitude but opposite in direction in the two wires, while the CM currents i_{cm} are equal in magnitude and have the same direction in both wires [1]. These noise current components must be driven by their respective noise sources. Figure 2.5 shows a HF equivalent circuit for the conducted emissions measurement set-up, which was shown in Figure 2.2. Note that it is not accurate to use the two Thévenin equivalent sources together in the same circuit. This is the reason for the dashed lines connecting the DM noise source in Figure 2.5. For the sake of simplicity, it has been assumed that the LISNs for the phase and the neutral are identical and provide 50Ω impedances with respect to ground.

Using the above definition of CM and DM currents, it is obvious from Figure 2.5 that the ground current i_g is twice the i_{cm} :

$$i_g = i_p + i_n = 2i_{cm} \quad (2.3)$$

Defining the DM and CM currents as in (2.2) is probably the reason why many authors define the DM voltage as:

$$v_{dm} = 50\Omega \cdot i_{dm} = \frac{50\Omega \cdot i_p - 50\Omega \cdot i_n}{2} = \frac{v_p - v_n}{2} \quad (2.4)$$

and the CM voltage as:

$$v_{cm} = 50\Omega \cdot i_{cm} = \frac{50\Omega \cdot i_p + 50\Omega \cdot i_n}{2} = \frac{v_p + v_n}{2} \quad (2.5)$$

From (2.4) and (2.5) one could deduce that the DM and CM voltages are equal to the

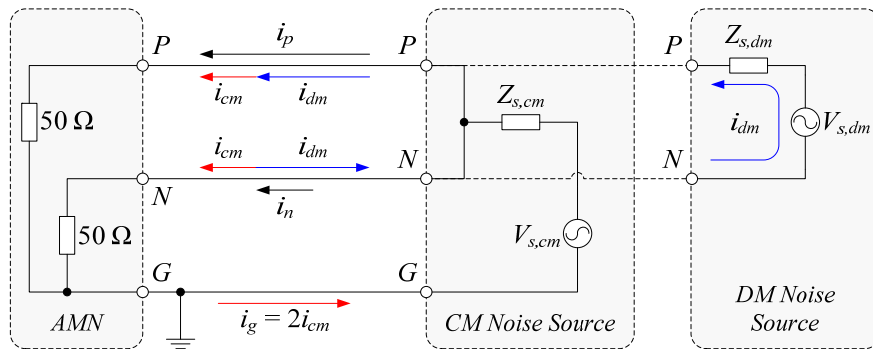


Figure 2.5: HF equivalent of the conducted emissions measurement circuit.
Drawing the CM and DM noise sources together would be inaccurate.

voltage drop of the corresponding currents across a 50Ω resistor.

According to a second school of thought, e.g. [3] and [11], the CM current is the sum of the phase and neutral currents:

$$i_{cm} = i_p + i_n \quad (2.6)$$

Then $i_{cm} = i_g$, but more importantly, i_{cm} is not necessarily equal in the phase and neutral wires. This definition is more plausible because the CM current is the unintended result of parasitic effects, such as stray capacitances, which depend on the physical layout and grounding. For instance, the effect of rapidly changing voltage v_c across a parasitic capacitance to ground C_p is a current:

$$i_c = C_p \frac{dv_c}{dt} \quad (2.7)$$

which flows to the ground. In a practical circuit, it is highly unlikely that the phase and neutral impedances to ground will be equal. As a consequence, the ground current is not equally split between the phase and the neutral. Therefore, a more appropriate equivalent circuit is the one in Figure 2.6, which is in agreement with the definition in (2.6).

Despite different definitions of CM current, the definition of CM voltage is same:

$$v_{cm} = \frac{v_p + v_n}{2} \quad (2.8)$$

In the case of conducted emissions testing, with the previous assumption of 50Ω resistances to ground, the relationship between the CM voltage and current is:

$$v_{cm} = \frac{v_p + v_n}{2} = \frac{50\Omega \cdot i_p + 50\Omega \cdot i_n}{2} = \frac{50\Omega}{2} (i_p + i_n) = 25\Omega \cdot i_{cm} \quad (2.9)$$

which can be interpreted as if the CM current i_{cm} sees two 50Ω resistances in parallel, i.e. 25Ω , and this is independent of how i_{cm} splits between the phase and the neutral.

The definition of the DM current is the same in both schools of thought:

$$i_{dm} = \frac{i_p - i_n}{2} \quad (2.10)$$

But the second school of thought defines the DM voltage differently:

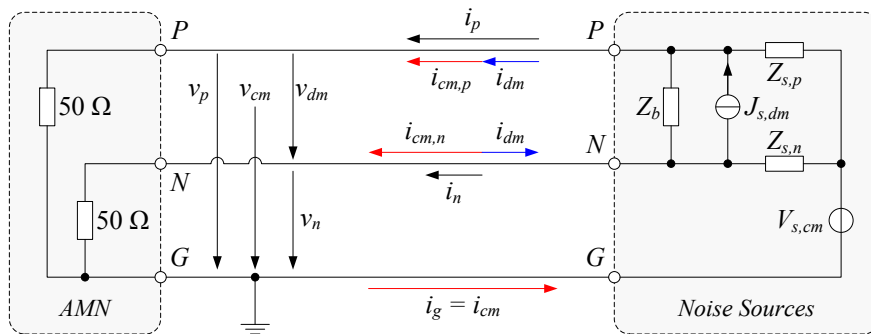


Figure 2.6: Another HF equivalent of the conducted emissions measurement circuit. Here a new noise source model and the second definition for CM and DM are used.

$$v_{dm} = v_p - v_n \quad (2.11)$$

When the noise currents are terminated by two 50Ω impedances to ground, as in the conducted emissions tests, the relationship between the DM voltage and current is:

$$v_{dm} = v_p - v_n = 50\Omega \cdot i_p - 50\Omega \cdot i_n = 2 \cdot 50\Omega \frac{i_p - i_n}{2} = 100\Omega \cdot i_{dm} \quad (2.12)$$

In other words, the DM voltage is the voltage drop over two 50Ω resistances in series (Figure 2.6), and therefore, the DM termination impedance is 100Ω .

2.4 Conducted Noise Separation

The components of a power filter attenuate CM and DM disturbances differently. For this reason, it is impossible to design or select an appropriate EMI filter without knowing the level of the CM and DM noise. Designers often lack knowledge or suitable tools to determine the amount of CM and DM noise and have to rely on a trial-and-error approach to achieve the desired noise suppression.

If a suitable current probe is available, the CM or DM conducted emissions can be measured as shown in Figure 2.7. For given noise sources, the noise currents depend on their load. With its 50Ω impedance to ground the LISN provides repeatability of the measurements. Let the current probe be connected to the input port of a measuring instrument with input impedance Z_m . Depending on how the phase and neutral wires go through the probe, the instrument can measure two different voltages:

$$V_{cm,m} = \frac{(\overline{I_p} + \overline{I_n}) \cdot Z_m}{n} \quad V_{dm,m} = \frac{(\overline{I_p} - \overline{I_n}) \cdot Z_m}{n} \quad (2.13)$$

where n is the turns ratio of the current probe. The CM and DM noise voltages can be solved by taking the sum of I_p and I_n from (2.9) and their difference from (2.12) and inserting them into (2.13):

$$V_{cm,m} = \frac{(\overline{I_p} + \overline{I_n}) \cdot Z_m}{n} = \frac{2V_{cm} Z_m}{n \cdot 50} \Rightarrow V_{cm} = \frac{n \cdot 50}{2Z_m} V_{cm,m} \quad (2.14)$$

$$V_{dm,m} = \frac{(\overline{I_p} - \overline{I_n}) \cdot Z_m}{n} = \frac{V_{dm} Z_m}{n \cdot 50} \Rightarrow V_{dm} = \frac{n \cdot 50}{Z_m} V_{dm,m} \quad (2.15)$$

In most cases, the input impedance of the measuring instrument, e.g. a spectrum analyzer, is $Z_m = 50 \Omega$, i.e. the same as the output impedance of a LISN in the MHz range. Then, at least for that range, (2.14) and (2.15) simplify to:

$$V_{cm} = \frac{n}{2} V_{cm,m} \quad V_{dm} = n V_{dm,m} \quad (2.16)$$

All current probes affect the measured circuit to some degree. Using a current probe is analogous to inserting an impedance $Z_{i,cp}$ in series with the load, which in this case is

To fulfill this criterion a noise separator must have 50 Ω input impedances, independent of input voltages, currents, or other factors. If this requirement is not fulfilled, the noise currents will differ from those in the standard conducted emissions measurement set-up, where both the CM and DM noise currents see 50 Ω to ground. How much they would change depends on the source impedances, which are unknown. The unknown change in the noise currents means an unknown error in the CM and/or DM voltage that is being measured. Unfortunately, many of the proposed reference designs have input impedances that depend on the input voltages.

- 3) The CM and DM components in the input signals must be passed to the corresponding output undistorted.

This requirement can be evaluated from the *DM transmission ratio* (DMTR):

$$DMTR = \frac{V_{o,dm}}{V_{i,dm}} \quad (2.19)$$

and the *CM transmission ratio* (CMTR):

$$CMTR = \frac{V_{o,cm}}{V_{i,cm}} \quad (2.20)$$

The $V_{o,dm}$ and $V_{o,cm}$ in (2.19) and (2.20) are the output voltages at the DM and CM outputs respectively. Ideally, a DM voltage $V_{i,dm}$ applied to the inputs should appear unchanged at the DM output, i.e. $V_{o,dm} = V_{i,dm}$. Similarly, a CM voltage $V_{i,cm}$ at the inputs should appear unchanged at the CM output, i.e. $V_{o,cm} = V_{i,cm}$. Therefore, ideally $DMTR = CMTR = 1$ for the respective outputs.

- 4) The unwanted mode signal must be attenuated as much as possible.

In order to evaluate this performance requirement, the *DM rejection ratio* (DMRR):

$$DMRR = \frac{V_{o,cm}}{V_{i,dm}} \quad (2.21)$$

and *CM rejection ratio* (CMRR):

$$CMRR = \frac{V_{o,dm}}{V_{i,cm}} \quad (2.22)$$

should be considered. Ideally, $DMRR = CMRR = 0$. Note that the rejection ratios characterize the output “opposite” to the input voltage mode, i.e. the voltage at the CM output should not be affected by the input DM voltage, and the DM output should not be affected by the input CM voltage.

All noise separators work by simultaneously adding and/or subtracting the noise voltages at the phase and neutral outputs of the AMN. Unfortunately, the commercially available LISNs for single-phase applications are not suited to working with noise separators. The reason is that they have only one RF output and a switch (see Figure 2.2), which determines whether the noise from the phase or the neutral is passed to the output. Therefore, in order to simultaneously add or subtract the noise signals, one has to:

- build an AMN with two RF outputs,
- modify a commercial AMN, or

- use two commercial AMN units simultaneously, which would require some work on the power cords at the inputs and outputs of the two units.

The first noise separator for single-phase applications known to the author was proposed by Clayton Paul [13] in 1988 and since then many solutions have been proposed [14]-[23]. Most of the separators use wideband HF transformers to perform simultaneous addition and subtraction of the noise signals [13]-[19]. Alternatively, these tasks can be performed with resistor networks [20]-[21], power combiners [22], or operational amplifiers [23].

The simplest noise separators are built with resistors [20]-[21] and perform the addition of the two input voltages. Therefore, they have only one output, which is supposed to give the CM voltage. That is why they may be called *DM rejection networks* (DMRNs) [20]. An example of such a resistive separator is shown in Figure 2.8a [21]. The problem with all such separators is that the impedances at both input ports depend on the voltages applied to them. For example, the noise separator shown in Figure 2.8a has input impedances:

$$Z_{in,p} = \frac{75 \cdot V_p}{2 \cdot V_p - V_n} \quad Z_{in,n} = \frac{75 \cdot V_n}{2 \cdot V_n - V_p} \quad (2.23)$$

which were derived in Appendix A.2.

The authors in [21] suggest the use of a wideband transformer for a 180° phase shift to obtain the DM noise. Unfortunately, this would not make the separator compliant with criterion 2) and would add parasitic couplings, which may only worsen its performance.

The power combiners have two inputs and one output, which provides either the sum or difference of the input signals (Figure 2.8b). They are commercially available RF circuits with matched ports, and therefore, criterion 2) is not an issue in this case. According to the results in [22] they have also very good transmission and rejection ratios, i.e. they fulfill criteria 3) and 4). Only criterion 1) is not fulfilled, because the 0° power combiner gives the sum of the input signals instead of (2.8). This is a minor disadvantage, because it can easily be corrected by subtracting 6 dB from the measured data:

$$V_{cm} [\text{dB}\mu\text{V}] = 20 \cdot \lg \left| \frac{\overline{V_p} + \overline{V_n}}{2} \right| = 20 \cdot \lg |\overline{V_p} + \overline{V_n}| - 20 \cdot \lg(2) \approx V_{cm,m} [\text{dB}\mu\text{V}] - 6 [\text{dB}] \quad (2.24)$$

Noise separators can also be built with operational amplifiers. The schematic of one such noise separator [23] is shown in Figure 2.8c. It is powered by batteries, not just for convenience, but also to prevent external EMI. To minimize the asymmetry, the inputs are buffered by op-amp voltage followers. The 50 Ω input impedances are achieved with 45 Ω resistors in series with 10 Ω trimmers. Additionally, two 10 pF trimmer capacitors are added across the input ports for better matching and compensation of eventual input cable and LISN asymmetries. The outputs of the voltage followers are passed to trivial summing and subtracting circuits. Finally, two 50 Ω resistors are added to the output of the circuit in order to halve the outputs, because [23] uses (2.4) and (2.5) as definitions for the DM and CM voltages. If the 50 Ω resistor from the DM output is removed, the circuit would be fully compliant with criterion 1). Criterion 2) is also satisfied, and according to the measurements in [23], this separator performed very well in terms of criteria 3) and 4) as well. On the negative side, noise separators with operation-

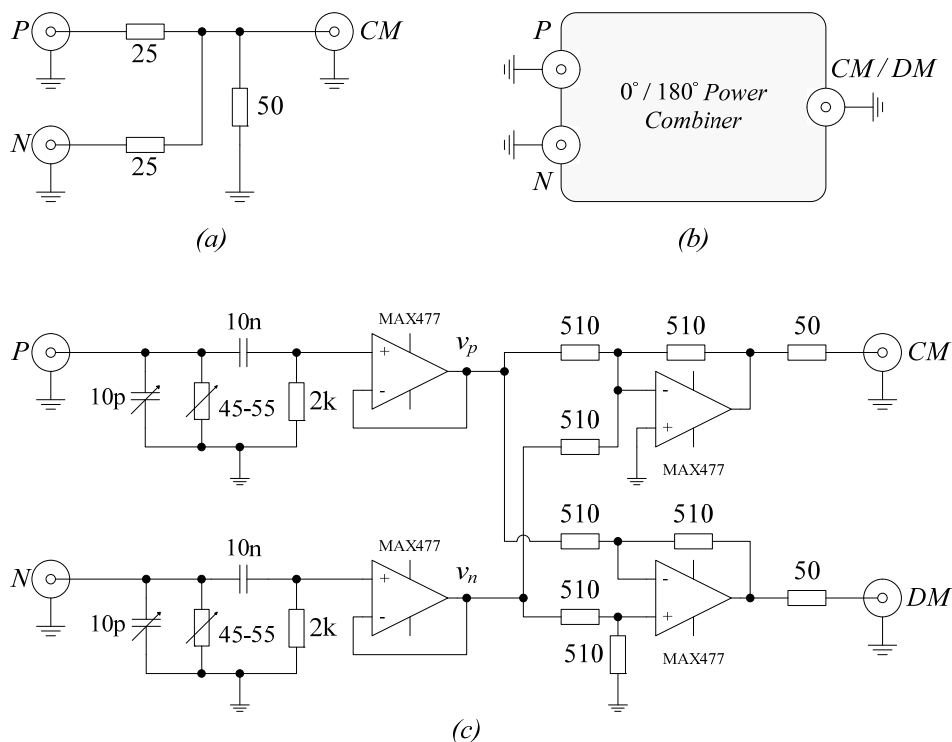


Figure 2.8: Examples of different types of noise separators:

a) Resistor-based DMRN [21]; b) power combiner; c) noise separator with operational amplifiers [23].

al amplifiers require a separate energy supply, they cannot be as robust as devices that use only passive components, and it is very difficult to achieve good performance up to 30 MHz with operational amplifiers.

The majority of separator designs use wideband transformers, including the oldest noise separator [13] by Clayton Paul, shown in Figure 2.9a. It suffers from the same disadvantage as the resistor-based noise separators: its input impedances are voltage dependent as shown in Appendix A.2.

The same problem can be found in the transformer-based separators proposed in [14], [15], [17], and [18]. The first transformer-based design which overcomes the input impedance issue was proposed by Andreas Nagel in 1999 [16]. The R_{cm} and R_{dm} in his circuit (Figure 2.9b) should be 25 Ω and 100 Ω respectively, but their practical realization in conjunction with the 50 Ω output port terminations is not shown and might lead to wrong implementations. The measurements in [16] show very good transmission and rejection ratios, except in the 10-30 MHz range, where the performance somewhat deteriorates as a result of the parasitics. In [17] and [18] Nagel's design was compared with a separator, shown in Figure 2.9c and very similar to Clayton's circuit. Not surprisingly, the circuit in Figure 2.9c also has voltage dependent input port impedances as shown in Appendix A.2.

The authors in [17] and [18] rightfully point out the importance of the parasitics for the performance of the separator and in order to minimize them, they did not use the *double pole - double throw* (DPDT) switch that is shown in Figure 2.9a and c. Instead, they built two devices – one for the CM and another for the DM noise.

Shuo Wang’s separator in Figure 2.9d [19] is an improved version of Nagel’s circuit, where the secondary winding of T1 is removed. This eliminates the parasitic capacitance between the primary and secondary windings. Another improvement is the use of a transmission line transformer. As a result the DMRR reported in [19] remains less than -60 dB up to 30 MHz. The CMRR is also very good. It is less than -60 dB up to about 15 MHz, but remains less than -50 dB up to 30 MHz. These data demonstrate excellent performance in terms of criteria 3) and 4). The input impedance criterion is also satisfied, if both outputs are terminated with 50 Ω . From the circuit in Figure 2.9d the realization of R_{cm} and R_{dm} in Nagel’s circuit (Figure 2.9b) is clearer. The only disadvantage is that the DM output should be corrected according to (2.18), because Wang defines the DM voltage as (2.4).

After this overview of separator technologies, it can be concluded that the best options are: current probes with appropriate characteristics, power combiners, or Wang’s separator with a transmission line transformer.

2.5 Noise Source Impedance

The noise source impedance is important for the performance of an EMI filter, and not surprisingly, it has been the topic of a number of publications [24]-[30]. The oldest of these references [24], suggests a resonance method to determine the noise source impedance Z_s . The same paper also points out that impedance measurement methods based

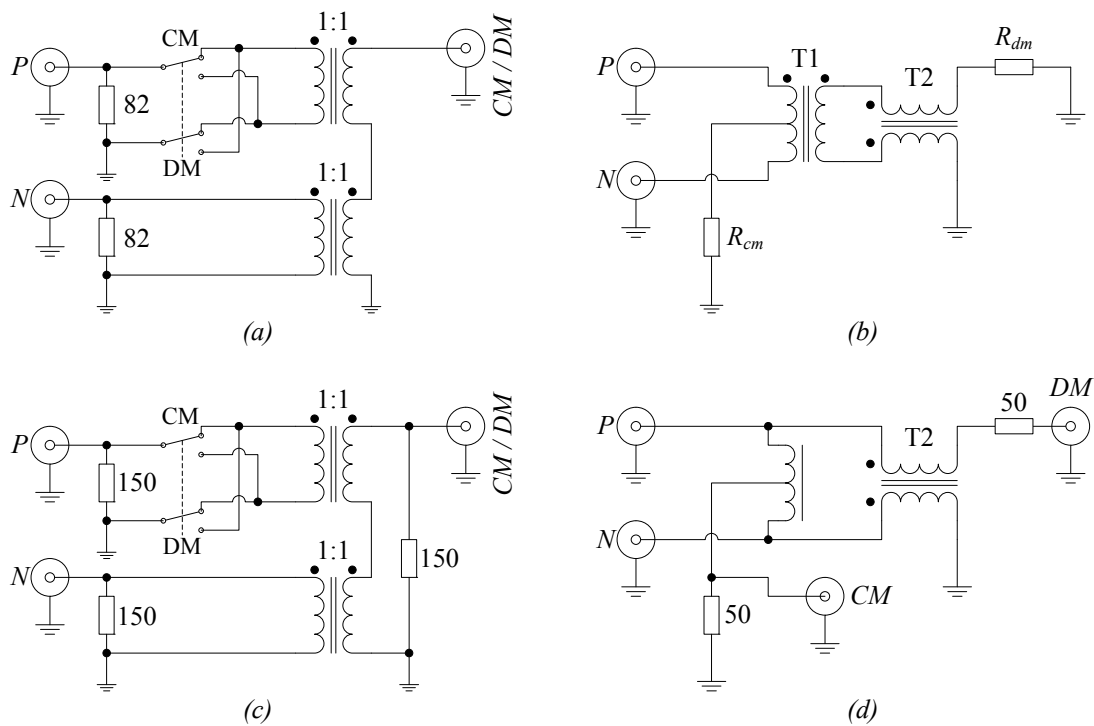


Figure 2.9: Wideband transformer-based noise separator designs:

a) by Clayton Paul [13], b) Andreas Nagel [16], c) Chiadò Caponet [17]-[18], and d) Shuo Wang [19].

on injected signal are not suitable for the task. Despite that, in [25]-[26], a method with two current probes was proposed, where one of the probes injects a test signal and the other measures the current, which depends on the circuit's impedance. The fundamental issue with this method is that what is obtained in the end is actually the input impedance of the EUT, which may or may not be the same as the noise source impedance. Unless one demonstrates that the input impedance of the EUT and its noise source impedance are the same it would be wrong to use any injection method.

Apart from the very laborious resonant method, among the published methods, there seems to be only one theoretically sound alternative – the IL method for measuring the noise source impedance. It was proposed by Zhang et al. [27] and uses the IL of known series and shunt components. The difficulty in this method is to determine the phase of the noise source impedance. The authors of the IL method suggest using Hilbert transform [31] to obtain the phase of the source impedance.

The methods in [28]-[29] also use series and shunt components with known characteristics. The noise source impedance is found with MATLAB's *fft* and *tfestimate* functions (*tfestimate* was *tfe* before MATLAB R14). The *tfestimate* function returns a transfer function estimate. Two of its arguments are the input and output signals of the system, but the output data must be the response of the system to the input data. Although [29] mentions only the *fast Fourier transform* (FFT), i.e. Matlab's *fft* function, the problem in both [28] and [29] is that the noise source impedances are obtained as ratios of the data obtained in two separate measurements, which is theoretically flawed.

The issues related to the noise source impedances can be explained using Figure 2.6. Both the CM and the DM noise are caused by the switching actions in a SMPC, but the mechanism of their creation is different. The DM current drawn by the SMPC pulsates as a result of the turning on and off of the power switch(es). The exact waveform depends on the topology of the converter, as discussed in Publication III, but it can be affected by a number of factors, such as snubbers, components, and parasitics. Whatever the waveform shape, the point is that for all converters operating with fixed switching frequency, the input current is a repetitive waveform and as such, it has a discontinuous spectrum, consisting of harmonics with frequencies that are multiples of the switching frequency. Therefore, the DM noise source is quite close to an ideal current source, which implies infinitely large DM noise source impedance ($Z_{s,dm}$). This contradicts the reported results in [27]-[29] according to which the $Z_{s,dm}$ is considerably smaller than the CM noise source impedance ($Z_{s,cm}$). According to [29] the $Z_{s,dm}$ does not exceed several tens of ohms, while $Z_{s,cm}$ is above several hundred ohms in the 0.15-30 MHz range. The most obvious reason for this contradiction is the large DC input capacitor, which is present in most converter topologies. Even if the DM noise source impedance were infinite, when it is shunted with a large capacitor, the source impedance seen at the input of the EUT will be the impedance of that capacitor itself. In Figure 2.6 the impedance of that capacitor is denoted by Z_b . Snubbers and other parts of the converter circuit might also contribute to Z_b . The parasitic impedances to ground ($Z_{s,p}$ and $Z_{s,n}$) are usually associated with $Z_{s,cm}$, but, as shown in Figure 2.6, they also affect the $Z_{s,dm}$:

$$Z_{s,dm} = Z_b \parallel (Z_{s,p} + Z_{s,n}) = \frac{Z_b (Z_{s,p} + Z_{s,n})}{Z_b + Z_{s,p} + Z_{s,n}} \quad (2.25)$$

In Publication III the DM noise source was assumed to be an ideal current source. The input capacitor was included in the analysis, but $Z_{s,p}$ and $Z_{s,n}$ were not. That is $Z_{s,dm} = Z_b$ was assumed, which is a mistake. The DM noise that should be expected with these assumptions was much larger than the measured one. One reason could be the failure to include $Z_{s,p}$ and $Z_{s,n}$, which would have led to lower $Z_{s,dm}$. Another reason for the discrepancy could be the input impedance of the SMPC itself ($Z_{in,c}$), which might be a part of $Z_{s,dm}$, but that is an open question. If it is, (2.25) should be modified to include $Z_{in,c}$:

$$Z'_{s,dm} = Z_b \parallel (Z_{s,p} + Z_{s,n}) \parallel Z_{in,c} \quad (2.26)$$

If that is the case, there would be no reason to object to the injection impedance measurement methods, and the method with two current probes described in [25]-[26] can be used to measure $Z_{s,dm}$. However, if $Z_{in,c}$ is not a part of the DM noise source impedance, then injection methods are not permissible for measuring $Z_{s,dm}$.

Unlike the DM, the CM noise is the result of the pulsating voltage across the parasitic impedance to ground. As seen from Figure 2.6, the CM noise source impedance is:

$$Z_{s,cm} = Z_{s,p} \parallel Z_{s,n} = \frac{Z_{s,p} Z_{s,n}}{Z_{s,p} + Z_{s,n}} \quad (2.27)$$

If $Z_{s,p} = Z_{s,n}$ then

$$Z'_{s,cm} = \frac{Z_{s,p}}{2} = \frac{Z_{s,n}}{2} \quad (2.28)$$

and the ground current would split equally between the phase and neutral wires.

If the Thévenin equivalent of the CM noise source model consists of an ideal voltage source and $Z_{s,cm}$, which depend only on $Z_{s,p}$ and $Z_{s,n}$, it may seem that injection methods can be used to measure the CM noise source impedance because there is no difference between it and the CM input impedance. However, the phase and neutral wires cannot be shorted while the SMPC is operating. Therefore, the method with two current probes [25]-[26] would work only if $Z_{s,p} = Z_{s,n}$, or if there is Z_b and it is much smaller than both $Z_{s,p}$ and $Z_{s,n}$. In general, i.e. when $Z_{s,p} \neq Z_{s,n}$ the measured CM impedance is not exactly $Z_{s,cm}$ because it includes Z_b (Figure 2.6).

The parasitic impedances to ground are predominantly capacitive. Their resistive components are so large, that they can be ignored and $Z_{s,cm}$ is often replaced by a capacitance. An interesting and simplified deduction of the CM noise source equivalent circuit for flyback, buck, boost, and buck-boost converters is given in [30] where the parasitic impedances to ground are assumed to be pure capacitances.

3 Passive Power Filters

EMI filters can be active or passive. Active filters are in fact power electronic converters, which inject the opposite of the noise current into the power line. As a result the unwanted current components are eliminated from the line current. Active power filters have a fundamentally different topology and operation and are not considered in this thesis. This chapter considers the circuits for single-phase EMI filters, their CM and DM equivalents, and the discrete components used in these filters.

3.1 Topology

Most power filters are passive low-pass filters with some distinctive features. An example of an EMI filter is shown in Figure 3.1a, inserted between the AMN and EUT, as it would be in the conducted noise test set-up. For simplicity, the output of the AMN is represented by its two $50\ \Omega$ impedances to ground. The filter in Figure 3.1a is a two-stage filter comprising the most important suppression components: X- and Y-capacitors, DM inductors, and a CM choke.

The topology of the filter should be selected by considering the required suppression and expected filter terminations. Depending on the source and load impedances there are four possible filter configurations [3]: T, π , LC, or CL configuration. These basic configurations, or stages, are repeated several times to achieve the necessary suppression. The performance of filters with a higher number of stages is less dependent on the source and load impedances. However, every stage also adds to the cost and size of the filter, which is why in most cases EMI filters have one or two stages.

The topology of the filter in Figure 3.1a is fairly common, despite the fact that power line impedances are usually unknown, or vary widely. In conducted compliance tests, the LISNs serve as loads providing two $50\ \Omega$ impedances to ground, which are enough to justify an X-capacitor at the output of the filter.

The topology at the input side depends on the noise source impedances. Some industry application notes stress that the Y-capacitors should be as close to the SMPC as possible. This makes sense, given the relatively high $Z_{s,cm}$. The DM noise source was earlier described as a current source, which calls for an X-capacitor at the input. Most SMPC have a large input capacitor, which could be seen as an X-capacitor, but if the input “bulk” capacitor does not have good HF characteristics, it is better to have a good suppression capacitor, such as C_{XI} in Figure 3.1.

Even if $Z_{s,dm}$ is a small, which would reduce the effectiveness of C_{XI} as a DM noise suppressor, the C_{XI} would still help in balancing the filter. Without the input capacitors, the two C_Y and C_{XI} in Figure 3.1, the CM currents would flow asymmetrically (depending on $Z_{s,p}$ and $Z_{s,n}$) through the phase and neutral terminals of the filter and degrade its performance.

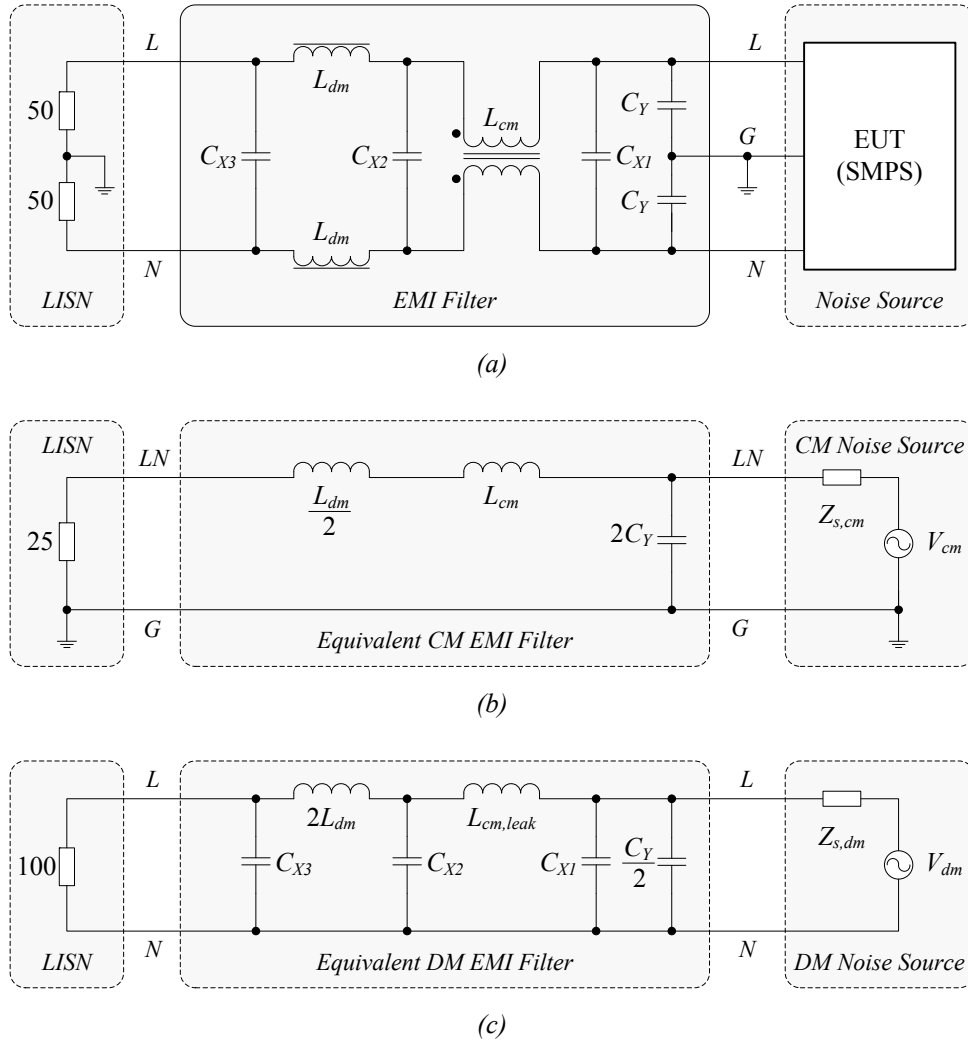


Figure 3.1: A two-stage passive power filter with its equivalent circuits:
 a) electrical circuit of the filter in compliance tests; b) HF CM equivalent circuit;
 c) HF DM equivalent circuit.

3.2 Equivalent Circuits

The CM and DM equivalent circuits of the filter in Figure 3.1a are shown in Figure 3.1b and c respectively. These are important for the design of power filters because the suppression capabilities of an EMI filter can be calculated from its CM and DM equivalent circuits. It will be shown later that the IL of the filter depends on its termination impedances. At least in conducted emissions testing the load impedances are known. As it was explained in Section 2.3, because of the AMN, the load for the CM noise is 25 Ω and for the DM noise it is 100 Ω. The source impedances were discussed in Section 2.5 and are the most uncertain elements in the equivalent circuits.

The equivalent circuits reveal that the X-capacitors attenuate only the DM noise, whereas the Y-capacitors suppress both CM and DM, but are more effective against the CM noise. The two decoupled DM inductors also attenuate both modes, but are more effective against the DM noise. The CM chokes are intended for CM noise suppression, but as shown in Appendix A.4, their leakage inductance contributes to the suppression of the DM noise. The CM and DM inductances of coupled DM inductors (there are no such in Figure 3.1) are also derived in Appendix A.4.

It is worth stressing that using coupled DM or two equal DM inductors is recommended because it makes the filter circuit symmetrical. The DM equivalent circuit in Figure 3.1c supports the widely-held view that an asymmetrical topology with a single inductor of double inductance on one of the lines would have the same effect as the symmetrical topology. In [32] it was shown that two 600 μH inductors performed better than a single 1200 μH inductor and this fact was one of the pieces of evidence for the so-called mixed-mode phenomenon. Depending on the CM and DM definitions (Section 2.3), the mixed-mode phenomenon can be interpreted differently: if the CM currents in both power lines are believed to be equal, then, in addition to the DM and CM components, there must be a third component, called mixed-mode in [32], to explain the phenomenon. However, if the CM currents in the phase and neutral conductors can differ as a result of unequal noise source impedances to ground, i.e. when $Z_{s,p} \neq Z_{s,n}$, then the phenomenon described is only the imbalance caused by the diode rectifier. In the light of the 2nd CM definition, the phenomenon can be seen as one of the causes for the discrepancy between $Z_{s,p}$ and $Z_{s,n}$.

Whether the noise source is symmetrical or not, there are two ways to reduce the imbalance between the phase and neutral lines. The first is to connect capacitors with good HF characteristics at the input of the filter, these are C_{Xl} and both C_Y , in Figure 3.1a, which ideally should short-circuit the phase and neutral wires at HF. If that would be the case, regardless of $Z_{s,p}$ and $Z_{s,n}$, if the impedances seen after the short-circuit point are equal, the ground current would split equally between the phase and neutral wires, i.e. $I_{cm,p} = I_{cm,n}$. The other way is to have equal and large series impedances on the phase and neutral wires. The LISN's 50 Ω impedances to ground will turn the series impedances into large and equal impedances to ground. If the phase- and neutral-to-ground impedances are equal and much larger than the $Z_{s,p}$ and $Z_{s,n}$, then $I_{cm,p} \approx I_{cm,n}$, even without input capacitors. In contrast, an asymmetrical filter circuit would make $I_{cm,p} \neq I_{cm,n}$, and may be the reason for exceeding the limits at either the phase or neutral. This is why in conducted emissions tests a seemingly equivalent symmetrical filter will always perform better than an asymmetrical one.

3.3 Components

Passive EMI filters, the subject of this thesis, consist of passive components: resistors, capacitors, and inductors. Each can have specific current and/or rating requirements, but they all must have good HF characteristics. As a result of the ever present parasitics any suppression component resonates at some frequency, namely the *self-resonant frequency* (SRF), given by:

$$f_{SRF} = \frac{1}{2\pi\sqrt{LC}} \quad (3.1)$$

where L and C are component's inductance and capacitance. For a resistor both of these are parasitic. For capacitors and inductors one of these is intrinsic, while the other is a parasitic parameter. Capacitors and inductors resemble their names only up to a third of their SRF [3] and above it the parasitic effects can no longer be ignored. Furthermore, above resonance a capacitor behaves like an inductor, and an inductor behaves like a capacitor. This is important because the SRF of most suppression capacitors and inductors falls within the 0.15 to 30 MHz range. For all passive components a higher SRF is an indicator of good HF characteristics, because it is the result of smaller parasitics. However, the quality of a component should not be judged only by its SRF. It is important also that its characteristics are independent of, for example, the load current, temperature, or aging. A suppression component must fulfill certain rating, safety, or other requirements as well.

3.3.1 Resistors

Resistors are rarely used in passive power filters. Although they could provide a high impedance path for the noise, just as inductors do, they would do the same to the mains frequency current, which would lead to unacceptable losses. Therefore, resistors are used only in combination with capacitors or inductors for special purposes, such as damping [33], impedance matching networks [3], or the cancellation of the *equivalent series resistance* (ESR) of a capacitor [34].

3.3.2 Capacitors

For low-frequency and DC signals, such as the supply currents in AC or DC power lines, a capacitor appears as high impedance, but for HF signals, such as the noise currents in the 0.15 to 30 MHz range, it is low impedance. This is why capacitors are connected in parallel with the noise source – they attenuate the conducted EME by shunting them.

Capacitors that are connected between phase and neutral are called X-capacitors. According to the equivalent circuits in Figure 3.1, they attenuate only the DM noise components. Because X-capacitors are not subject to safety restrictions, their capacitance can be whatever suits the design and their voltage rating depends on the line voltage.

Suppression capacitors, connected from phase or neutral to ground, are called Y-capacitors. They are subject to strict safety regulations and must be capable of withstanding very high voltages. For instance, in single-phase applications powered by 230 Vac, they have to be rated at 2 kV. The values of Y-capacitors are limited by the permitted leakage current. Although Y-capacitors are intended for CM noise suppression, they help in the attenuation of DM noise as well.

Feedthrough capacitors are a special type of suppression capacitors. Unlike other capacitors, these are three-terminal devices. The connecting wires pass through the capacitor

structure. For this reason feedthrough capacitors have not only voltage, but also current ratings. Thanks to their special structure, feedthrough capacitors have minimal parasitic inductance and a much higher SRF than other types of capacitors.

The equivalent circuit of a capacitor [3] is shown in Figure 3.2a. The *equivalent parallel resistance* (EPR) is very large and is often ignored, as in Figure 3.2b, where the remaining parasitics are the ESR and *equivalent series inductance* (ESL). The ESL is the reason for a capacitor to resonate and to appear as an inductor above the SRF. The ESR is the impedance of the capacitor at resonance.

It is well known that both the ESL and ESR can be reduced by more than half (because smaller capacitors have smaller parasitics) by connecting two equal capacitors in parallel. However, it is even more effective to connect them diagonally as proposed in [34] and illustrated in Figure 3.2c. The impedance of each of the two capacitors in the figure is denoted by Z_c and the impedances of the connections between them are assumed equal and denoted by Z_{PCB} . This constitutes a symmetrical diagonal connection, which in Appendix A.3 is shown to have an equivalent symmetrical T-circuit as in Figure 3.2d.

Assuming that $Z_{PCB} = R_{PCB} + j\omega L_{PCB}$, it follows that:

$$\frac{Z_c - Z_{PCB}}{2} = \frac{1}{j\omega 2C} + j\omega \frac{L_{ESL} - L_{PCB}}{2} + \frac{R_{ESR} - R_{PCB}}{2} \quad (3.2)$$

When $Z_{PCB} = 0$ is equivalent to the trivial parallel connection of two capacitors, where the capacitance doubles, while L_{ESL} and R_{ESR} are halved. However, if $L_{PCB} = L_{ESL}$ and $R_{PCB} = R_{ESR}$, the advantages of the diagonal connection are most obvious, because the parasitics are canceled and the two diagonally connected capacitors behave like an ideal capacitor. In practice that is impossible because, firstly, a capacitor's parasitics are subject to tolerances, just like its capacitance, and secondly, these parasitics, as well as L_{PCB} and R_{PCB} , vary with temperature, frequency, and current.

The ESL of suppression capacitors is so small that L_{PCB} of similar magnitude can be achieved on the PCB tracks connecting the two capacitors. The authors of [34] provide the approximate equation for a rectangular PCB winding, but other track geometries can be used as well. Most modern PCB design software applications have tools that can calculate the inductance of a PCB track, which aids the implementation of a capacitor's

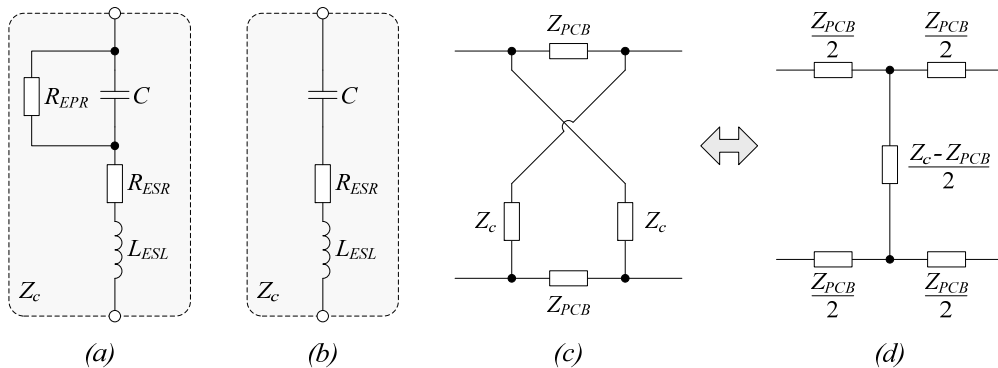


Figure 3.2: Capacitor's equivalent circuits and parasitics cancellation:

- a) capacitor's equivalent circuit; b) capacitor's equivalent circuit with EPR ignored; c) diagonal connection of two equal capacitors with equal impedances between the connections;
- d) symmetrical T-equivalent of the diagonal circuit in c).

ESL cancellation during the PCB design stage. The effort to match L_{PCB} to L_{ESL} is worthwhile, because the SRF can be increased significantly, which improves the HF performance of the capacitor, and consequently, that of the entire filter.

The ESR depends on the type and size of the capacitor. It is small, but usually not as small as the resistance of the PCB track. Therefore, in order to cancel the ESR, two discrete resistors have to be inserted – one on each PCB track connecting the two capacitors. This, of course, will minimize the ESR, but the benefit is much smaller than ESL cancellation. In most applications, the use of cancellation resistors does not look worthwhile: an increased component count, increased PCB complexity, and reduced efficiency – all these disadvantages against a marginal benefit of minimizing the ESR, which would be reduced anyway, just by using diagonal connection without any cancellation resistors.

3.3.3 Inductors

Unlike capacitors, suppression inductors provide a low impedance path for mains frequency signals, and high impedance for HF signals. For this reason, inductors are connected in series with the noise and power sources. Suppression chokes have some serious disadvantages: they are bulky, they have large tolerances, and their HF characteristics are sensitive to changes in the temperature or current (because the nominal inductance drops as a result of the saturation of the core). Finally, they may act as antennae emitting and picking up radiated EME. Despite these shortcomings EMI filters do have at least one inductor. This is mostly because Y-capacitor values are limited for safety reasons and the required CM attenuation must be achieved mainly by the inductive components of the filter.

There are two types of suppression inductors: DM and CM chokes. In comparison with capacitors, inductors have more non-linear characteristics and resonate at lower frequencies. Nevertheless, the linear equivalent circuits in Figure 3.3 are traditionally used in the analysis and design of EMI filters. The most detailed circuit in Figure 3.3a reveals that similarly to a capacitor, an inductor has ESR and EPR, but it also has *equivalent parallel capacitance* (EPC), which spoils the HF characteristics of an inductor. The EPR is often ignored, as in Figure 3.3b, because it is relatively large. In contrast, the ESR is small, but sometimes it can also be ignored (Figure 3.3c) because from the suppression point of view it does no harm. The problem with the ESR is that it heats the inductor and reduces the efficiency. Heat-related problems are a big headache for electronics designers, but what is relevant from the EMC perspective, is that the heating af-

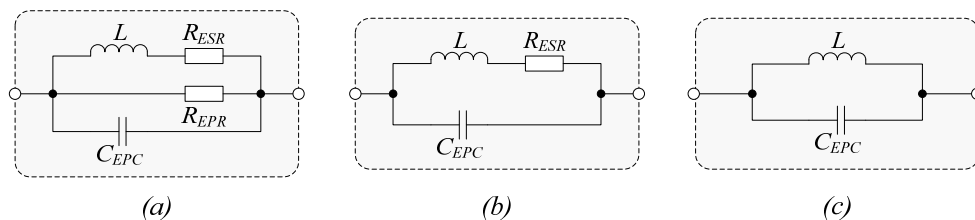


Figure 3.3: Equivalent circuits for two-terminal inductor:

a) according to [43]; b) according to [3]; c) simplified equivalent circuit with ESR and EPR ignored.

fects the inductor's characteristics, and thus, its suppression performance. The third parasitic element, the EPC, represents the total effect of the turn-to-turn and turn-to-core parasitic winding capacitances of the inductor.

In order to improve the HF characteristics and suppression performance of an inductor, its EPC must be minimized. The obvious way to achieve this is to reduce the turn-to-turn parasitic capacitance by increasing the distance between the turns, but that would increase the size of the inductor. It is much better to use some of the EPC cancellation techniques described in [35]-[39]. The essence of EPC cancellation for two separate (decoupled) DM inductors is again in the diagonal connection (Figure 3.4a). In Appendix A.3, it is shown that the symmetrical diagonal connection (Figure 3.4b) has a symmetrical π -equivalent as in Figure 3.4c. Therefore, assuming

$$\left. \begin{aligned} Y_c &= j\omega C_c \\ Y_{ind} &= \frac{1}{j\omega L} + j\omega C_{EPC} \end{aligned} \right\} \Rightarrow Y_{ind} - Y_c = \frac{1}{j\omega L} + j\omega(C_{EPC} - C_c) \quad (3.3)$$

It can be seen from (3.3) that the diagonally connected cancellation capacitors C_c appear as X-capacitors, and the capacitive part of the admittances along each line can be zero in theory if $C_c = C_{EPC}$, i.e. the cancellation capacitors must be selected so as to be equal to the EPC of the inductors. As with the capacitors' ESL cancellation, perfect EPC cancellation is impossible in practice because there is asymmetry between the two inductors, all parameters of the inductors and cancellation capacitors have tolerances, and they all vary with frequency and temperature.

CM choke coils (Figure 3.5a) in single-phase applications are four-terminal devices. It is hard to distinguish them from coupled DM inductors (Figure 3.5b) as both consist of two windings on a common core, like a 1:1 transformer, but the couplings between the windings are opposite. Unlike transformers, CM chokes and coupled DM inductors do not provide galvanic isolation.

The equivalent circuits that are usually shown in textbooks (Figure 3.3) are not suitable for four-terminal inductors. The derivation of the CM and DM inductances for two ideal coupled inductors is shown in Appendix A.4. In the analysis of real coupled inductors, each winding can be replaced by one of the models for two-terminal inductors. In addi-

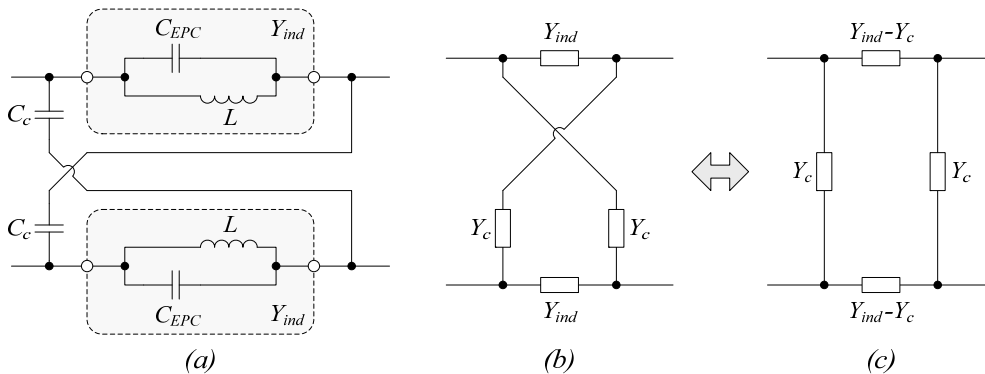


Figure 3.4: EPC cancellation for decoupled DM inductors:

- a) two decoupled DM inductors with their EPC and diagonally connected cancellation capacitors C_c ;
- b) symmetrical diagonal circuit; c) symmetrical π -equivalent of the symmetrical diagonal circuit.

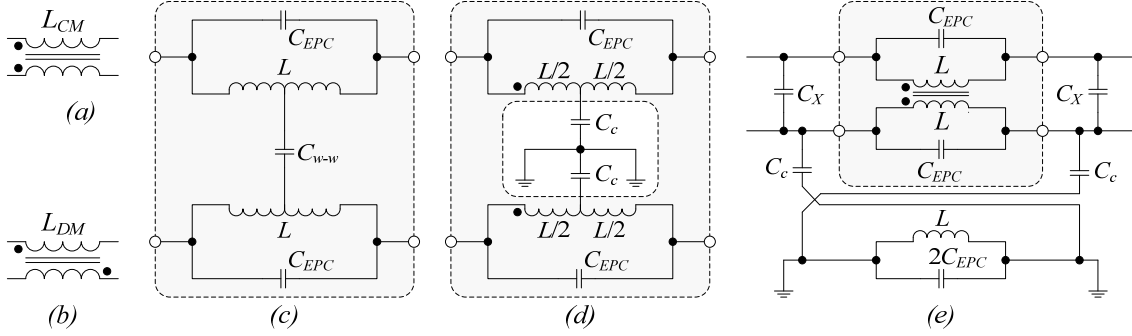


Figure 3.5: EPC cancellation for CM chokes:

a) CM choke; *b)* coupled DM inductors; *c)* coupled inductors (can be CM or DM) with their EPC and parasitic winding-to-winding capacitance C_{w-w} ; *d)* EPC cancellation for CM chokes; *e)* another method for CM choke EPC cancellation.

tion to that, one more parasitic capacitance, the winding-to-winding capacitance C_{w-w} in Figure 3.5c, must be considered.

The parasitic C_{w-w} does not affect the CM inductance, which is why for CM chokes only the EPC has to be minimized. One method for EPC cancellation for integrated CM filters was introduced in [37]. The same method was applied to discrete CM inductors in [39]. The idea of the method is to connect a capacitor between the center tap of each winding and the ground as shown in Figure 3.5d. If $C_c = 4C_{EPC}$, the transfer impedance in the π -equivalent of the T-circuit will have no capacitive component, i.e. the EPC would be cancelled. In [39], a second method for EPC cancellation of CM chokes is suggested (Figure 3.5e), but it is less appealing, because in addition to the two C_c , it would also require an inductor on the ground path, with certain L and C_{EPC} values.

The parasitic C_{w-w} complicates the EPC cancellation for coupled DM inductors. Depending on the values of C_{w-w} and C_{EPC} , [39] suggests two different cancellation schemes:

- 1) If $\frac{C_{w-w}}{2} < C_{EPC}$, use diagonal connection (Figure 3.6a) with $C_c = C_{EPC} - \frac{C_{w-w}}{2}$

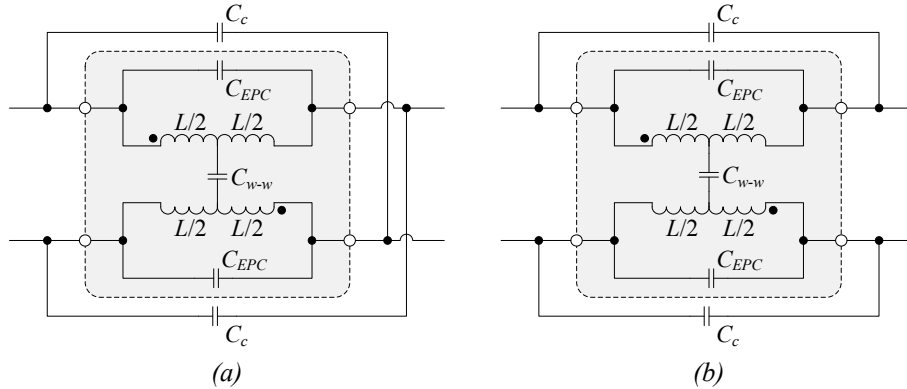


Figure 3.6: EPC cancellation for coupled DM inductors:

a) by diagonal connection, *b)* by parallel connection.

2) If $\frac{C_{w-w}}{2} > C_{EPC}$, use parallel connection (Figure 3.6b) with $C_c = \frac{C_{w-w}}{2} - C_{EPC}$

The above EPC cancellation techniques can significantly improve the HF characteristics of suppression inductors at the cost of only two small capacitors. Although complete EPC cancellation is impossible, the SRF of inductors can be increased significantly. SRFs of over 20-30 MHz are reported in [38]-[39]. To the best of the author's knowledge, there are no commercially available suppression inductors yet that use EPC cancellation. Therefore, it is up to the engineers who design passive power filters to implement the EPC cancellation techniques. For that they need accurate information about the characteristics of the inductors which they are going to use in the filter. Publication VII shows how to obtain the CM and DM characteristics of four-terminal inductors from the measurements of their network parameters.

4 Characterization and Design of Power Filters

The CISPR 17 standard prescribes methods for the measurement of the IL of passive RF suppression filters, which may consist of single elements, such as capacitors, inductors, or resistors, or their combinations in either the lumped or distributed types [40]. As a consequence, passive power filters are traditionally characterized by their IL. The IL is a good indicator of a filter's suppression capabilities, but only for a given set of conditions. Using the IL data alone, there is no way to predict a filter's performance when the termination or loading conditions change. Network parameters serve much better as characterization tools because when they are known any electrical characteristic can be found, regardless of the source and load impedances. The following section focuses on the IL and its definition, measurement and relationship with the two-port and four-port network parameters. In Section 4.2, the network parameters are used to obtain the elements of the CM and DM π -equivalent circuits of a single-phase power filter. If needed, the π -equivalent circuits can be transformed to their T-equivalent. Finally, in Section 4.3, the most important design steps are outlined.

4.1 Insertion Loss

Most textbooks define the IL as the ratio, in dB, of two powers in accordance with the following equation:

$$IL = 10 \cdot \lg \left(\frac{P_{20}}{P_2} \right), \text{ dB} \quad (4.1)$$

where P_{20} is the power delivered to the load impedance Z_L , which in a measurement set-up is the input impedance of the measurement instrument's receiver, connected to the signal generator as in Figure 4.1a. P_2 is the power delivered to the same impedance by the same generator, but with a filter inserted between them, as shown in Figure 4.1b. In the same figure, V_1 and V_2 are, respectively, the input and output voltages of the filter. Similarly, I_1 and I_2 denote the input and output current. Ideally $V_{10} = V_{20}$ and $I_{10} = -I_{20}$

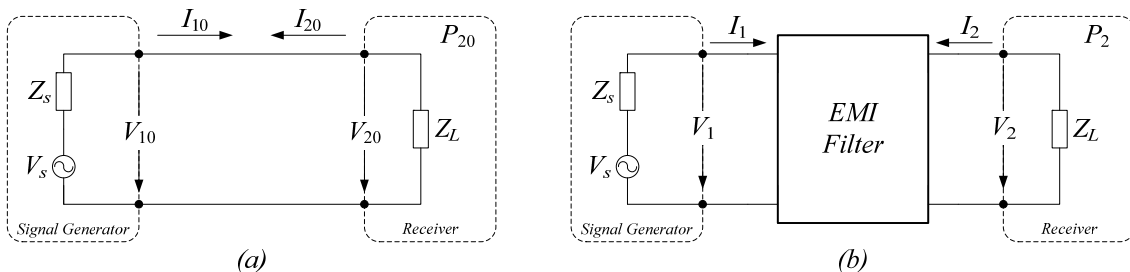


Figure 4.1: Insertion loss definition:

a) reference measurement (filter replaced by short circuit); *b)* measurement with the filter inserted. The direction of the output current is irrelevant in the definition of IL. Here it is selected so as to match the definition used in the two- and n -port networks.

in the reference measurement (Figure 4.1a).

In CISPR 17, the IL is defined as the ratio of the voltages appearing across the line immediately beyond the point of insertion, before and after the insertion of the filter [40]. Similarly, the oldest textbook definition [41] known to the author defines the IL as the insertion ratio IR in dB:

$$IR = \frac{V_{20}}{V_2} = \frac{I_{20}}{I_2} \Rightarrow IL = 20 \cdot \lg(IR) = 20 \cdot \lg\left(\frac{V_{20}}{V_2}\right) = 20 \cdot \lg\left(\frac{I_{20}}{I_2}\right) \quad (4.2)$$

In Publications V and VI it was shown that definition (4.1) is equivalent to (4.2):

$$IL = 10 \cdot \lg\left(\frac{P_{20}}{P_2}\right) = 20 \cdot \lg\left(\frac{I_{20}}{I_2}\right) = 20 \cdot \lg\left(\frac{V_{20}}{V_2}\right) \quad (4.3)$$

It is worth noting that both definitions above require the source and load impedances (Z_s and Z_L) to be the same in both measurements - with and without a filter. They do not require Z_s and Z_L to be resistive, equal to each other, or constant.

CISPR 17 specifies that in the standard IL measurements the input and output of the filter must be terminated in equal and fixed resistances - normally 50Ω to 75Ω [40]. When $Z_s = Z_L$ the load voltage $V_{20} = V_s/2$ and (4.3) becomes:

$$IL' = 20 \cdot \lg\left(\frac{V_s}{2V_2}\right) \quad (4.4)$$

Obviously (4.4) is a special case, but not equivalent to the classical IL definition (4.3). Other definitions of IL [42] are not considered in this thesis. Ambiguous definitions and superficial consideration given to (4.3) and (4.4) are probably the reasons for confusing the IL with voltage attenuation. However, the latter is a ratio of the filter's input and output voltages, which does not depend on the source impedance, only on the load. In contrast, the IL depends on both the source and load impedances.

There are also different notions of the worst case IL. It is natural to think of it as the theoretical minimum IL provided by a suppression filter or component. However, in CISPR 17 it is defined as the IL measured in $0.1 \Omega / 100 \Omega$ and the reverse systems. In Publication V the minimum IL is shown to be the smaller of the c_{11} and c_{22} chain parameters of the filter or component.

4.1.1 Insertion Loss in Terms of Two-Port Parameters

The IL of a two-port device can be expressed in terms of different sets of two-port parameters. With the notations used in Appendix A.1.2 the IL equations given in the literature are:

- Chain c -parameters [3]:

$$IL = 20 \cdot \lg \left| \frac{c_{11}Z_L + c_{22}Z_s + c_{12} + c_{21}Z_sZ_L}{Z_s + Z_L} \right| \quad (4.5)$$

- Impedance z -parameters [3]:

$$IL = 20 \cdot \lg \left| \frac{(Z_s + z_{11})(Z_L + z_{22}) - z_{12}z_{21}}{(Z_s + Z_L)z_{21}} \right| \quad (4.6)$$

- Scattering s -parameters [43]:

$$IL = 20 \cdot \lg \left| \frac{(1 - \rho_s s_{11})(1 - \rho_L s_{22}) - \rho_s \rho_L s_{12} s_{21}}{(1 - \rho_s \rho_L) s_{21}} \right| \quad (4.7)$$

where ρ_s and ρ_L are the source and load reflection coefficients, defined as:

$$\rho_s = \frac{Z_s - Z_0}{Z_s + Z_0} \quad \text{and} \quad \rho_L = \frac{Z_L - Z_0}{Z_L + Z_0} \quad (4.8)$$

If needed, the IL in terms of other two-port network parameters can be derived with the aid of the conversion tables found in various textbooks, such as [44].

When $Z_s = Z_L = Z_0$, (4.5) and (4.6) do not simplify significantly, but (4.7) becomes:

$$IL' = 20 \cdot \lg \left| \frac{1}{s_{21}} \right| = -20 \cdot \lg |s_{21}| \quad (4.9)$$

because $\rho_s = \rho_L = 0$.

4.1.2 Insertion Loss in Terms of Four-Port Parameters

By definition, the IL is applicable to two-port networks, but most filters have a higher number of ports. Single-phase power filters are four-port networks and measurements of their suppression characteristics require one measurement for the CM, as shown in Figure 4.2a, and another for the DM IL (Figure 4.2b). Both of these measurements transform the four-port network into a two-port one. Instead of altering the circuit of the filter, the CM or DM IL can be calculated from its four-port parameters. The test circuit for measuring the four-port s -parameters is shown in Figure 4.2c. The equations for IL in terms of four-port network parameters are derived and verified in Publication VI. The CM IL in terms of four-port admittance y -parameters is shown to be:

$$IL_{cm} = 20 \cdot \lg \left| \frac{Z_s Z_L}{Z_s + Z_L} \left[\frac{y_{12} + y_{14} + y_{32} + y_{34} - \left(y_{11} + y_{13} + y_{31} + y_{33} + \frac{1}{Z_s} \right) \left(y_{22} + y_{24} + y_{42} + y_{44} + \frac{1}{Z_L} \right)}{(y_{21} + y_{23} + y_{41} + y_{43})} \right] \right| \quad (4.10)$$

And the DM IL in terms of four-port impedance z -parameters is:

$$IL_{dm} = 20 \cdot \lg \left| \frac{z_{12} - z_{14} - z_{32} + z_{34} + \left(z_{11} - z_{13} - z_{31} + z_{33} + Z_s \right) \left(z_{24} - z_{22} + z_{42} - z_{44} - Z_L \right)}{z_{21} - z_{23} - z_{41} + z_{43}} \right| \quad (4.11)$$

Both the CM and DM IL can also be expressed in terms of four-port scattering s -parameters by inserting into (4.7) the so-called mixed-mode s -parameters [11]:

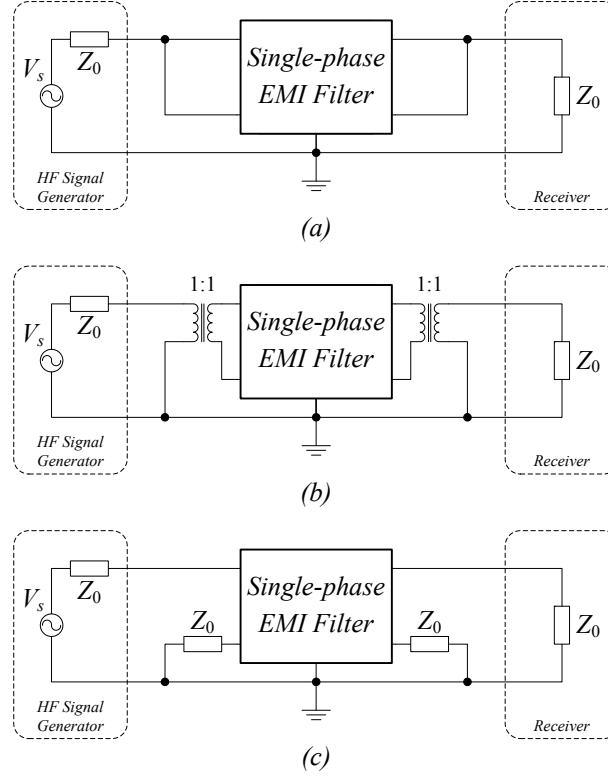


Figure 4.2: Measurement test circuits:
a) for CM IL measurement (asymmetrical); b) for DM IL measurement (symmetrical);
c) for four-port s -parameters measurement.

$$\mathbf{S}_{mm} = \begin{bmatrix} \mathbf{S}_{cc} & \mathbf{S}_{cd} \\ \mathbf{S}_{dc} & \mathbf{S}_{dd} \end{bmatrix} \quad (4.12)$$

where \mathbf{S}_{mm} is the mixed-mode s -matrix, i.e. a 4×4 matrix, consisting of four 2×2 sub-matrices. The \mathbf{S}_{cc} sub-matrix contains the CM s -parameters, obtained from the standard four-port s -parameters as follows:

$$\mathbf{S}_{cc} = \begin{bmatrix} S_{cc11} & S_{cc12} \\ S_{cc21} & S_{cc22} \end{bmatrix} = \frac{1}{2} \begin{bmatrix} S_{11} + S_{13} + S_{31} + S_{33} & S_{12} + S_{14} + S_{32} + S_{34} \\ S_{21} + S_{23} + S_{41} + S_{43} & S_{22} + S_{24} + S_{42} + S_{44} \end{bmatrix} \quad (4.13)$$

The \mathbf{S}_{dd} sub-matrix in (4.12) contains the DM s -parameters, which also come from the single-ended four-port s -parameters:

$$\mathbf{S}_{dd} = \begin{bmatrix} S_{dd11} & S_{dd12} \\ S_{dd21} & S_{dd22} \end{bmatrix} = \frac{1}{2} \begin{bmatrix} S_{11} - S_{13} - S_{31} + S_{33} & S_{12} - S_{14} - S_{32} + S_{34} \\ S_{21} - S_{23} - S_{41} + S_{43} & S_{22} - S_{24} - S_{42} + S_{44} \end{bmatrix} \quad (4.14)$$

The remaining two sub-matrices \mathbf{S}_{cd} and \mathbf{S}_{dc} in (4.12) represent the cross-mode s -parameters. They are also 2×2 matrices and for symmetrical networks should theoretically be zero, but in practice this is impossible because the two sides of the network cannot be perfectly balanced.

The reference impedance for the CM s -parameter matrix \mathbf{S}_{cc} is half of the reference impedance of the single-ended four-port s -parameters. Therefore, if the reference imped-

ance for the measured single-ended s -parameters is $Z_0 = 50 \Omega$, the reference impedance for \mathbf{S}_{cc} is 25Ω and the CM IL for arbitrary termination is:

$$IL_{cm} = 20 \cdot \lg \left| \frac{(1 - \rho_s s_{cc11})(1 - \rho_L s_{cc22}) - \rho_s \rho_L s_{cc12} s_{cc21}}{(1 - \rho_s \rho_L) s_{cc21}} \right| \quad (4.15)$$

However, this time ρ_s and ρ_L are:

$$\rho_s = \frac{Z_s - Z_0/2}{Z_s + Z_0/2} \quad \text{and} \quad \rho_L = \frac{Z_L - Z_0/2}{Z_L + Z_0/2} \quad (4.16)$$

The reference impedance of the DM s -matrix \mathbf{S}_{dd} is twice that of its source matrix, i.e. if the reference impedance for the measured single-ended s -parameters is $Z_0 = 50 \Omega$, the reference impedance for \mathbf{S}_{dd} is 100Ω . Then the DM IL in terms of mixed-mode s -parameters is:

$$IL_{dm} = 20 \cdot \lg \left| \frac{(1 - \rho_s s_{dd11})(1 - \rho_L s_{dd22}) - \rho_s \rho_L s_{dd12} s_{dd21}}{(1 - \rho_s \rho_L) s_{dd21}} \right| \quad (4.17)$$

where ρ_s and ρ_L are:

$$\rho_s = \frac{Z_s - 2Z_0}{Z_s + 2Z_0} \quad \text{and} \quad \rho_L = \frac{Z_L - 2Z_0}{Z_L + 2Z_0} \quad (4.18)$$

In the special case when $Z_s = Z_L = Z_0$, from (4.10) the CM IL becomes:

$$IL'_{cm} = 20 \cdot \lg \left[\frac{\frac{Z_0}{2} \left[\begin{array}{l} y_{12} + y_{14} + y_{32} + y_{34} - \\ \left(y_{11} + y_{13} + y_{31} + y_{33} + \frac{1}{Z_0} \right) \left(y_{22} + y_{24} + y_{42} + y_{44} + \frac{1}{Z_0} \right) \end{array} \right]}{(y_{21} + y_{23} + y_{41} + y_{43})} \right] \quad (4.19)$$

Or in terms of s -parameters from (4.15) and (4.16) it follows that:

$$\rho_s = \rho_L = \frac{1}{3} \Rightarrow IL'_{cm} = 20 \cdot \lg \left| \frac{(3 - s_{cc11})(3 - s_{cc22}) - s_{cc12} s_{cc21}}{8s_{cc21}} \right| \quad (4.20)$$

From (4.11) the DM IL for the special case when $Z_s = Z_L = Z_0$ is:

$$IL'_{dm} = 20 \cdot \lg \left| \frac{\begin{array}{l} z_{12} - z_{14} - z_{32} + z_{34} + \\ \left(z_{11} - z_{13} - z_{31} + z_{33} + Z_0 \right) \left(z_{24} - z_{22} + z_{42} - z_{44} - Z_0 \right) \\ + \\ z_{21} - z_{23} - z_{41} + z_{43} \end{array}}{2Z_0} \right| \quad (4.21)$$

Finally, from (4.17) and (4.18) the DM IL can also be given in terms of s -parameters:

$$\rho_s = \rho_L = -\frac{1}{3} \Rightarrow IL'_{dm} = 20 \cdot \lg \left| \frac{(3 + s_{dd11})(3 + s_{dd22}) - s_{dd12} s_{dd21}}{8s_{dd21}} \right| \quad (4.22)$$

4.2 CM and DM Π -equivalent Circuits

If the s -parameters of a two-port network (Figure 4.3a) are known, then the transfer impedance Z in its π -equivalent circuit (Figure 4.3b) is:

$$Z = \frac{R_0 [(1 + s_{11})(1 + s_{22}) - s_{12}s_{21}]}{2s_{21}} \quad (4.23)$$

And the Y_1 and Y_2 admittances in Figure 4.3b are:

$$Y_1 = \frac{(1 - s_{11})(1 + s_{22}) + s_{12}s_{21} - 2s_{21}}{R_0 [(1 + s_{11})(1 + s_{22}) - s_{12}s_{21}]} \quad Y_2 = \frac{(1 + s_{11})(1 - s_{22}) + s_{12}s_{21} - 2s_{21}}{R_0 [(1 + s_{11})(1 + s_{22}) - s_{12}s_{21}]} \quad (4.24)$$

Equations (4.23) and (4.24) could be expressed in terms of any other type of two-port network parameters. In fact they were derived in Publication VII using the c -parameters of a π -circuit (Publication I). It should also be noted that (4.23) and (4.24) are valid for reciprocal networks, which have $s_{12} = s_{21}$. Although networks containing anisotropic materials, such as ferrites, are non-reciprocal, the measurements of various passive filters and components, e.g. the measurements of a CM choke in Publication VI, show that at least in a small-signal sense they appear as reciprocal networks.

In Chapter 3 the CM and DM equivalent circuits of the filter were discussed and an example was shown in Figure 3.1. No matter how complex the topology of the filter is, it can be replaced by one π -circuit for CM and another for DM. The elements of these two equivalent circuits can be calculated from (4.23) and (4.24) by inserting either the CM or the DM s -parameters, which can be measured directly or indirectly. The direct measurements are performed in the asymmetrical and symmetrical test circuits – the same test circuits that were shown in Figure 4.2a and b with regard to the CM and DM IL measurements. The starting point of the indirect measurements is the four-port network parameters, from which the two-port CM and DM parameters can be calculated. Because of the proliferation of VNAs the original measured data are usually the four-port s -parameters, which are converted to mixed-mode s -parameters, as explained in the previous section.

The main advantages of the direct method are its simplicity and widespread use. The main disadvantages are the use of auxiliary networks and the consequent errors. The direct method is simple when a four-port VNA is used. Four-port s -parameters can be measured also with a two-port VNA, but then measurements must be performed between all port pairs, while the remaining two ports are terminated with the same reference impedance as that of the VNA. The main advantage of the indirect method is that there is no need for auxiliary networks and thus it is free of the associated errors. How-

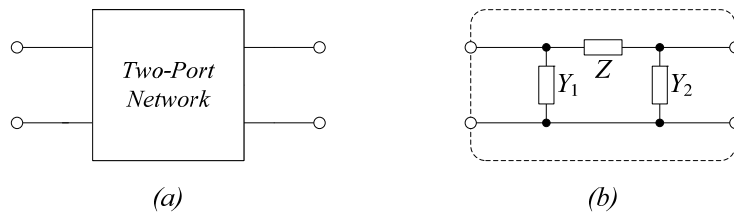


Figure 4.3: a) A general two-port network; b) π -equivalent circuit.

ever, there is a conversion error when converting from single-ended to mixed-mode s -parameters. Although the magnitude of that error is unknown, it will be the same regardless of the place and time of conversion – it depends only on the random measurement errors in the original measurement. In contrast, the errors in the direct measurements contain not only the inevitable random measurement errors, but also the errors resulting from the use of auxiliary networks. The latter are caused by unspecified wiring and balun circuits used in different laboratories around the world. Therefore, the repeatability of indirect CM and DM IL or s -parameter measurements cannot be achieved by direct measurements.

4.3 EMI Filter Design

Whether different authors emphasize different aspects of the design, or whether each application has its specific requirements, the fact is that there are many criteria and procedures for EMI filter design given in the literature, e.g. [3]-[4], [33], [45]-[50]. Publication IV falls in the same group because it suggests a procedure for designing the input filters for DC-DC converters. The large number of design procedures can be confusing, but it is possible to outline several design steps that must be part of any procedure if one wishes to avoid guesswork. Depending on the specific application, some modifications or additional steps might be necessary.

4.3.1 Determine the CM and DM Suppression Requirements

This is an important step, because without knowing the required suppression it is impossible to design the EMI filter. Some design procedures do not even mention such a step. In others, it is a required design parameter, but they do not explain where the required attenuation, or IL, comes from. Probably the first reference that addressed this point is [33], according to which the required CM and DM attenuation is obtained by subtracting the limit from the emissions. In Publication II the required IL was related to the definition of IL:

$$IL = 10 \cdot \lg\left(\frac{P_{20}}{P_2}\right) = 20 \cdot \lg\left(\frac{V_{20}}{V_2}\right) = 20 \cdot \lg(V_{20}) - 20 \cdot \lg(V_2) \quad (4.25)$$

To have the noise voltage with EMI filter below certain limit means that the second term in (4.25) must not exceed that limit. Then replacing that term with the limit would give the required IL. Unfortunately, this is not so simple because the limits are for the total noise in any of the two power lines, but the designers need to have IL requirements for CM and DM separately.

If the SMPS has already been built, the CM and DM noise can be measured with the aid of one of the noise separators discussed in Section 2.4. However, when the EMI filter design goes in parallel with the converter design, the noise cannot be measured. In most cases the design of the SMPC and its input filter go simultaneously, because it would cost more if the converter has to be redesigned because of problems with its input filter.

For example, the filter might turn out to be too large, or it may affect the SMPC badly; it can even make it unstable.

If the converter is not ready and the CM and DM noise cannot be measured, they can be estimated by simulations or calculations, but at least the converter topology and its operating voltages and currents must be known (Publication III). The main difficulty in this case is to predict the CM noise currents, because they depend on the CM noise source impedances, which are hard to measure even from a ready SMPC.

The correct suppression requirements for the CM and DM parts of the filter can be derived from the maximum noise voltage at the phase and neutral ($V_{p/n,\max}$), which should not exceed the limit line in the standard. When the CM and DM voltages are defined as in (2.4) and (2.8), the maximum noise voltage $V_{p/n,\max}$ is:

$$\left. \begin{array}{l} v_p = v_{cm} + v_{dm} \\ v_n = v_{cm} - v_{dm} \end{array} \right\} \Rightarrow v_{p/n} = v_{cm} \pm v_{dm} \Rightarrow V_{p/n,\max} = V_{cm} + V_{dm} \leq V_{\lim} \quad (4.26)$$

And when the DM voltage is defined as (2.11):

$$\left. \begin{array}{l} v_p = v_{cm} + v_{dm}/2 \\ v_n = v_{cm} - v_{dm}/2 \end{array} \right\} \Rightarrow v_{p/n} = v_{cm} \pm v_{dm}/2 \Rightarrow V_{p/n,\max} = V_{cm} + \frac{V_{dm}}{2} \leq V_{\lim} \quad (4.27)$$

If the CM noise voltage is specified to be one n^{th} of the limit, where $n > 1$, then the required CM IL can be given as:

$$IL_{cm,req} = 20 \cdot \lg(V_{cm,20}) - 20 \cdot \lg(V_{cm,2}) = 20 \cdot \lg(V_{cm,20}) - 20 \cdot \lg\left(\frac{V_{\lim}}{n}\right) \quad (4.28)$$

$$IL_{cm,req} = \text{CM noise without filter, [dB}\mu\text{V]} - \text{Limit, [dB}\mu\text{V]} + 20 \cdot \lg n$$

With the assumption that the CM noise is one n^{th} of the limit, and using (4.26), the DM noise voltage can also be expressed as a fraction of the limit:

$$V_{dm} = V_{p/n,\max} - V_{cm} \leq V_{\lim} - V_{cm} = V_{\lim} - \frac{V_{\lim}}{n} = V_{\lim} \frac{n-1}{n} \quad (4.29)$$

Then the required DM IL is:

$$IL_{dm,req} = 20 \cdot \lg(V_{dm,20}) - 20 \cdot \lg(V_{dm,2}) = 20 \cdot \lg(V_{dm,20}) - 20 \cdot \lg\left(V_{\lim} \frac{n-1}{n}\right) \quad (4.30)$$

$$IL_{dm,req} \approx \text{DM noise without filter, [dB}\mu\text{V]} - \text{Limit, [dB}\mu\text{V]} + 20 \cdot \lg\left(\frac{n}{n-1}\right)$$

For instance, if $n = 2$, i.e. when the design goal is to have CM and DM noise such that each does not exceed half of the standard limit, the required CM and DM IL are 6 dB above the difference from the corresponding noise voltages and the standard limit. However, $n = 2$ does not necessarily mean an optimum suppression-sharing between the CM and DM parts of the filter. Furthermore, when the DM noise voltages without a filter are obtained with a separator, or any method that defines the DM voltage as (2.11), then (4.30) is not accurate. From (4.27), with a CM noise voltage equal to one n^{th} of the limit, i.e. (4.28) is valid, the DM noise voltage is:

$$\frac{V_{dm}}{2} = V_{p/n, \max} - V_{cm} \leq V_{\lim} - V_{cm} \Rightarrow V_{dm} \leq 2 \left(V_{\lim} - \frac{V_{\lim}}{n} \right) = 2V_{\lim} \frac{n-1}{n} \quad (4.31)$$

Therefore, the required IL_{dm} is given by:

$$IL_{dm, req} = 20 \cdot \lg(V_{dm,20}) - 20 \cdot \lg(V_{dm,2}) = 20 \cdot \lg(V_{dm,20}) - 20 \cdot \lg \left(2V_{\lim} \frac{n-1}{n} \right) \quad (4.32)$$

$$IL_{dm, req} \approx \text{DM noise without filter, [dB}\mu\text{V]} - \text{Limit, [dB}\mu\text{V]} - 6 + 20 \cdot \lg \left(\frac{n}{n-1} \right)$$

Therefore, when the DM voltage is defined as in (2.11), the required DM IL is 6 dB lower than that calculated by (4.30). For the above example, when $n = 2$, that would mean the required CM IL is 6 dB above the difference between the CM noise without a filter and the standard limit, whereas the required DM IL is equal to the difference between the DM noise without a filter and the limit line in the standard.

4.3.2 Selecting Filter Topology

The topology should be selected according to the source and load impedances. However, for the reasons discussed in Sections 3.1 and 3.2, a symmetrical π -circuit is usually the best option. If the suppression requirements can be met with a single stage this is good, but often more stages are necessary. Contrary to the popular opinion, a multistage filter can have a smaller size and weight than a single-stage filter with the same IL. Another advantage of multistage filters is that their IL is less dependent on the source and load mismatch. The disadvantages of a multistage topology are possible resonances, which would require damping, and the parasitic couplings between the increased numbers of components of the filter.

The EMI filter topology changes significantly as a result of the diagonal and parallel connections, necessary for capacitor ESL and inductor EPC cancellation (Sub-sections 3.3.2 and 3.3.3 respectively). There are also methods for mutual parasitic coupling cancellation [51]-[52], which can add to the complexity of the circuit. For example, the “cancellation turn” [52] which is used for minimizing the mutual inductance between X-capacitors can be seen as another component of the filter, or at least it must be considered in the design of the PCB.

4.3.3 Selecting Filter Components

After the circuit of the filter has been selected, the component values in that circuit must be determined. The Y-capacitors can easily be determined from the leakage current limit [3], which is given in the safety standards applicable to the particular equipment. With known Y-capacitors, the CM inductance can be calculated from:

$$L = \frac{1}{4\pi^2 f_c^2 C} \quad (4.33)$$

where f_c should be the corner frequency, which can be defined as the intersection between the 0 dB line and a line with slope 40 dB/decade that is tangent to the required CM IL. Similarly, the DM corner frequency is determined from the required DM IL.

When the CM inductance is being calculated, the capacitance C in (4.33) should be twice the C_Y value, as seen from the equivalent circuit in Figure 3.1*b*. The CM inductance consists of the CM choke's inductance and half of the inductance of the DM inductors, if these are decoupled inductors. If the DM inductors are coupled, they have negligible CM inductance and then the CM inductor should have an inductance, equal to the required CM inductance, obtained by (4.33).

There is more freedom in the selection of the values for X-capacitors and DM inductors. One can try several combinations of capacitance and inductance values to find the smallest size or lowest price for a given DM corner frequency. The important point is that when all the component values are selected, the CM and DM equivalents of the filter must provide the required IL.

The selection of the filter components involves not just the calculation of suitable capacitance and inductance values, but also other considerations, such as inductor core material, the dielectric of the capacitor, voltage, and current ratings, the voltage drop at line frequency, size, weight, etc.

The network parameters are an excellent tool which can be applied at this stage of the design. They can be used to characterize single components as well as the entire filter. If the network parameters of the components are known, the entire filter can be characterized using c -parameters (Publication II) or transmission t -parameters. It should be remembered that this would not yield perfectly accurate results, because the network parameters of each component do not account for the influence of the neighboring components.

The topology of the filter and its component values can be helpful in the design of the controller of the SMPS. When a SMPC and its input filter are designed in parallel, some analytical checks and/or simulations can be performed at this point, so that at the end the system as a whole performs as desired. If the SMPS has already been built, and its controller cannot be changed, there is a risk that the dynamic performance of the converter can deteriorate after the input filter is added to it [53]-[55]. In some cases it may even become unstable.

4.3.4 Layout Design

When the topology and components of the filter have been selected, they have to be arranged on the PCB in compliance with the applicable safety regulations and in a way that minimizes the couplings between the components of the filter or other sources of radiated EME. At frequencies above several MHz the layout is the most critical step in the entire design procedure. A bad layout can spoil an otherwise appropriately sized filter. The following points summarize some of the recommendations for layout design found in various sources:

- 1) There is electromagnetic coupling between capacitors. To reduce it, there could be a sufficient distance left between the capacitors, they could be oriented so as

to be perpendicular to each other, or they could be shielded. The cancellation turn [52], which was mentioned earlier, is another technique for minimizing the coupling between two capacitors.

- 2) There is electromagnetic coupling between capacitors and inductors. The electromagnetic field around capacitors and inductors depends on their geometry and structure. Therefore, the coupling between capacitors and inductors can be affected by their orientation with respect to each other, by the distances between them, or shielding.
- 3) There is electromagnetic coupling between inductors. Again, it can be minimized by sufficient distance, perpendicular placement, or appropriate winding directions to get either positive or negative mutual inductance.
- 4) Different winding arrangements lead to different levels of radiated noise from inductors [51].
- 5) The areas of the input and output trace loops must be as small as possible to reduce the EMI that these trace loops induce in the components of the filter.
- 6) A ground plane under inductors increases their parasitic capacitance. Therefore, it is recommended to remove the ground plane under inductors.

4.3.5 Check Performance of the SMPS with Filter

When the filter prototype is ready, it has to be tested with the SMPS. The conducted and radiated emissions from the equipment must not exceed the limits set in the standards. For any manufacturer, it is important not only to pass the EMC norms, but also to have a product that performs well. Therefore, attention should be paid to how the SMPS copes with line and load changes. It was mentioned earlier that the dynamic characteristics of the SMPC change when an input filter is added at its input. This topic was partially treated in Publication I. Later it was studied in greater detail in [53]-[55] and other publications, but it is beyond the scope of this thesis.

All is well if the EUT passes the EMC requirements and performs as expected. Unfortunately, that is not always the case. If the EUT fails the conducted emissions tests in the lower part of the frequency spectrum, the required CM and/or DM IL must be increased, which may require an additional stage, or an increase in the L and C values. If the EUT fails the tests at higher frequencies, or in the radiated emissions tests, the emphasis should be on improving the layout and grounding of the filter. The use of shielding might also be considered. A possible remedy can be to use components with better HF characteristics. For example, if the Y-capacitors in the filter have a SRF about 10-20 MHz, they are inductive above that frequency, which could be the reason for failing the test in the 25-30 MHz. If that is the case, replacing the Y-capacitors with feedthrough capacitors, or applying the ESL cancellation techniques could solve the problem. Of course, if the test failure is due to parasitic couplings, using more expensive components will not help, but a better layout will.

5 Conclusions

This thesis reviewed some issues and recent developments in the design and characterization of passive single-phase power filters. It was pointed out that there are different definitions of CM and DM in the literature. Designers should be aware of these in order to understand the attenuation requirements or the data obtained with a noise separator.

From the overview of noise separation techniques, it can be concluded that resistive noise separators and some of the transformer-based designs are flawed. Noise separators with operational amplifiers have major disadvantages: a need for energy supply and low accuracy, because it would be difficult to achieve high CMRR with operational amplifiers. Therefore, to obtain the CM and/or DM noise it is recommended to use current probes compliant with CISPR-16-1-2, power combiners, or the circuits proposed by Nagel and Wang. Current probes and power combiners are commercially available and highly accurate. The Nagel and Wang separators are transformer-based circuits, with characteristics comparable to those of commercial power combiners. For highest accuracy it is recommended to use transmission line transformers.

Estimating the noise source impedance remains one of the most difficult issues in EMI filter design. Some of the measurement methods found in the literature are flawed and it is an open question whether injection methods are appropriate for this task. If they are not permissible, there are two options left: the resonant and IL methods, both of which are difficult to implement and time-consuming.

Network parameters were shown to be powerful tools for modeling and analysis of passive power filters and their components. Methods to obtain the CM and DM IL, the “worst-case” IL, and the CM and DM π -equivalent circuits in terms of two- and four-port network parameters were proposed. These methods can be used in the design or modeling of filters or their components.

It is impossible to list all the design procedures, recommendations, and improvement techniques found in the literature, but those that the author found most useful and relevant to the subject, were explained or referred to in the thesis. A novel method to obtain the required IL from the measured CM and DM noise was presented. Without knowing the required IL the designer has to guess the component values and oversize the filter.

Symmetrical filter circuits are strongly recommended. Recently published methods for improving the HF characteristics of capacitors and inductors by canceling their ESL and EPC were listed. The techniques for minimizing the electromagnetic couplings between the components of the filter were summarized as well. The theory explaining the interactions between a SMPC and its input filter is a topic of its own. Several references were given for those wishing to know more about these issues.

Finite element analysis can be considered for more accurate modeling and analysis of power filters. Although it is considerably more computationally intensive and time-consuming it is becoming more widespread. More research on noise source impedance and its measurement might give an insight into the nature of the noise sources and an-

swer the question about the applicability of injection methods. It may also lead to new, more practical and accurate noise source impedance measurement methods.

References

- [1] Paul R. Clayton: Introduction to Electromagnetic Compatibility, 2nd ed., John Wiley & Sons Inc., 2006, p. 983.
- [2] Tim Williams: EMC for Product Designers, 2nd edition, Reed Educational and Professional Publishing Ltd. 1996, p. 299.
- [3] László Tihanyi: Electromagnetic Compatibility in Power Electronics, IEEE Press, 1995, p. 403.
- [4] Richard L. Ozenbaugh: EMI Filter Design, Marcel Decker Inc., 1996, p. 252.
- [5] CISPR 16, Specification for radio disturbance and immunity measuring apparatus and methods – Part 2-1: Methods of measurement of disturbances and immunity – Conducted disturbance measurements, IEC, Genève, Switzerland, 2008.
- [6] CISPR 16, Specification for radio disturbance and immunity measuring apparatus and methods – Part 1-2: Radio disturbance and immunity measuring apparatus – Ancillary equipment – Conducted disturbances, IEC, Genève, Switzerland, 2006.
- [7] CISPR 16, Specification for radio disturbance and immunity measuring apparatus and methods – Part 1-1: Radio disturbance and immunity measuring apparatus – Measuring apparatus, IEC, Genève, Switzerland, 2006.
- [8] CISPR 11, Industrial, scientific and medical (ISM) radio-frequency equipment – Electromagnetic disturbance characteristics – Limits and methods of measurement, IEC, Genève, Switzerland, 2003.
- [9] CISPR 22, Information technology equipment – Radio disturbance characteristics – Limits and methods of measurement, IEC, Genève, Switzerland, 2006.
- [10] ISO/IEC Guide 98-3: 2008, Uncertainty of measurement – Part 3: Guide to the expression of uncertainty in measurement, ISO, Genève, Switzerland, 2008.
- [11] David E. Bockelman and W. R. Eisenstadt: *Combined differential and common-mode scattering parameters: theory and simulation*, IEEE Transactions on Microwave Theory and Techniques, Vol. 43, No. 7, July 1995, pp. 1530-1539.
- [12] Current Probe R&S[®]EZ-17, Rohde & Schwarz GmbH&Co., March, 2005.
- [13] Clayton R. Paul and K.B. Hardin: *Diagnosis and reduction of conducted noise emissions*, IEEE Transactions on Electromagnetic Compatibility, Vol. 30, No. 4, November, 1988, pp. 553–560.
- [14] K.Y. See and C.S. Ng: *Diagnosis of conducted interference with discrimination network*, International Conference on Power Electronics and Drive Systems, Singapore, February 21–24, 1995, pp. 433–437.
- [15] K.Y. See: *Network for conducted EMI diagnosis*, Electronics Letters, Vol. 35, No. 17, August 19, 1999, pp. 1446-1447.
- [16] Andreas Nagel and R.W. De Doncker: *Separating common mode and differential mode noise in EMI measurements*, EPE 1999, Lausanne, Switzerland, 1999, p. 8.

- [17] M.C. Caponet, F. Profumo, L. Ferraris, A. Bertoz, and D. Marzella: *Common and differential mode noise separation: comparison of two different approaches*, IEEE Power Electronics Specialists Conference, Vol. 3, June 17-21, 2001, pp. 1383-1388.
- [18] M.C. Caponet and F. Profumo: *Devices for the separation of the common and differential mode noise: design and realization*, IEEE Applied Power Electronics Conference, Volume 1, March 10-14, 2002, pp. 100-105.
- [19] Shuo Wang, F.C. Lee, and W.G. Odendaal: *Characterization, Evaluation, and Design of Noise Separator for Conducted EMI Noise Diagnosis*, IEEE Transaction on Power Electronics, Vol. 20, No. 4, July 2005, pp. 974-982.
- [20] Mark J. Nave: *A novel differential mode rejection network for conducted emissions diagnostics*, IEEE National Symposium on Electromagnetic Compatibility, May 23–25, 1989, pp. 223–227.
- [21] Hsin-Lung Su and Ken-Huang Lin: *Computer-aided design of power line filters with a low cost common and differential-mode noise diagnostic circuit*, IEEE International Symposium on Electromagnetic Compatibility, Vol. 1, August 13-17, 2001, pp. 511-516.
- [22] T. Guo, D.Y. Chen, and F.C. Lee: *Separation of the common-mode and differential-mode conducted EMI noise*, IEEE Transactions on Power Electronics, Vol. 11, No. 3, May 1996, pp. 480–488.
- [23] Tapani von Rauner: *A Measurement System for Evaluation of the Coupling Modes and Mechanisms of Conductive Noise*, Master's Thesis, Helsinki University of Technology, 1997, p. 64.
- [24] L.M. Schneider: *Noise Source Equivalent Circuit Model for Off-Line Converters and its Use in Input Filter Design*, Proceedings of Powercon 10, 1983, p. 11.
- [25] K.Y. See and L. Yang: *Measurement of Noise Source Impedance of SMPS Using Two Current Probes*, Electronics Letters, Vol. 36, No. 21, October 12, 2000, pp. 1774-1776.
- [26] K.Y. See and J. Deng: *Measurement of Noise Source Impedance of SMPS Using a Two Probes Approach*, IEEE Transactions on Power Electronics, Vol. 19, No. 3, May 2004, pp. 862-868.
- [27] D. Zhang, D.Y. Chen, M.J. Nave, and D. Sable: *Measurement of Noise Source Impedance of Off-Line Converters*, IEEE Transactions on Power Electronics, Vol. 15, No. 5, September 2000, pp. 820-825.
- [28] J. Meng, W. Ma, and L. Zhang: *Determination of Noise Source and Impedance for Conducted EMI Prediction of Power Converters by Lumped Circuit Models*, IEEE 35th Annual Power Electronics Specialists Conference, PESC'04, Aachen, Germany, June 2004, Vol. 4, pp. 3028-3033.
- [29] J. Meng, W. Ma, Q. Pan, Z. Zhao, and L. Zhang: *Noise Source Lumped Circuit Modeling and Identification for Power Converters*, IEEE Transactions on Power Electronics, Vol. 53, No. 6, December 2006, pp. 1853-1861.
- [30] C. Henglin, F. Limin, C. Wei, and Q. Zhaoming: *Modeling and Measurement of the Impedance of Common Mode Noise Source of Switching Converters*, IEEE

- 21st Annual Applied Power Electronics Conference, APEC'06, March 2006, pp. 1165-1168.
- [31] F.M. Tesche: *On the Use of the Hilbert Transform for Processing Measured CW Data*, IEEE Transactions on Electromagnetic Compatibility, Vol. 34, No. 3, August 1992, pp. 259-266.
- [32] S. Qu and D.Y. Chen: *Mixed-mode EMI Noise and Its Implications to Filter Design in Offline Switching Power Supplies*, IEEE Transactions on Power Electronics, Vol. 17, Issue 4, July 2002, pp. 502-507.
- [33] M.J. Nave: *Power Line Filter Design for Switched-Mode Power Supplies*, VanNostrand Reinolds Inc., 1991, p. 210.
- [34] S. Wang, F.C. Lee, and W.G. Odendaal: *Using a Network Method to Reduce the Parasitic Parameters of Capacitors*, IEEE 35th Annual Power Electronics Specialists Conference, PESC'04, Aachen, Germany, June 2004, Vol. 1, pp. 304-308.
- [35] T.C. Neugebauer, J.W. Phinney, and D.J. Perreault: *Filters and Components with Inductance Cancellation*, IEEE Transactions on Industry Applications, Vol. 40, No. 2, March/April 2004, pp. 483-491.
- [36] T.C. Neugebauer and D.J. Perreault: *Filters With Inductance Cancellation Using Printed Circuit Board Transformers*, IEEE Transactions on Power Electronics, Vol. 19, No. 3, May 2004, pp. 483-491.
- [37] R. Chen, J.D. van Wyk, S. Wang, and W.G. Odendaal: *Improving the characteristics of integrated EMI filters by embedded conductive layers*, IEEE Transactions on Power Electronics, Vol. 20, No. 3, May 2004, pp. 611-619.
- [38] S. Wang, F.C. Lee, and J.D. van Wyk: *Inductor Winding Capacitance Cancellation Using Mutual Capacitance Concept for Noise Reduction Application*, IEEE Transactions on Electromagnetic Compatibility, Vol. 48, No. 2, May 2006, pp. 311-318.
- [39] S. Wang, F.C. Lee, and J.D. van Wyk: *Design of Inductor Winding Capacitance Cancellation for EMI Suppression*, IEEE Transactions on Power Electronics, Vol. 21, No. 6, November 2006, pp. 1825-1832.
- [40] CISPR 17, *Methods of Measurement of the Suppression Characteristics of Passive Radio Interference Filters and Suppression Components*, IEC, Genève, Switzerland, 1981.
- [41] W.C. Johnson: *Transmission Lines and Networks*, McGraw-Hill Inc., 1950, p. 361.
- [42] S.M. Vakil: *MIL-STD-220A versus Classical Measurement of Filter Insertion Loss in a 50- Ω System*, IEEE Transactions on EMC, Vol. 25, November 1983, pp. 382-388.
- [43] L. Besser and R. Gilmore: *Practical RF Circuit Design for Modern Wireless Systems, Volume 1, Passive Circuits and Systems*, Artec House Inc., 2003, p. 539.
- [44] Guillermo Gonzalez: *Microwave Transistor Amplifiers Analysis and Design*, Prentice-Hall Inc., 1984, p. 245.

- [45] F.C. Lee and Y. Yu: *Input-Filter Design for Switching Regulators*, IEEE Transactions on Aerospace and Electronic Systems, Vol. AES-17, No. 5, September 1979, pp. 627-634.
- [46] S.Y. Erich and W.M. Polivka: *Input Filter Design Criteria for Current-Programmed Regulators*, IEEE Transactions on Power Electronics, Vol. 7, No. 1, January 1992, pp. 143-151.
- [47] F.-Y. Shih, D.Y. Chen, Y.-P. Wu, and Y.-T. Chen: *A Procedure for Designing EMI Filters for AC Line Applications*, IEEE Transactions on Power Electronics, Vol. 11, No. 1, January 1996, pp. 170-181.
- [48] V. Vlatković, D. Borojević, and F.C. Lee: *Input Filter Design for Power Factor Correction Circuits*, IEEE Transactions on Power Electronics, Vol. 11, No. 1, January 1996, pp. 199-205.
- [49] V. Grigore, J. Kyrrä, and J. Rajamäki: *Input Filter Design for Power Factor Correction Converters Operating in Discontinuous Conduction Mode*, IEEE International Symposium on EMC, Vol. 1, August 1999, pp. 145-150.
- [50] D.M. Mitchel: *Power Line Filter Design Considerations for DC-DC Converters*, IEEE Industry Applications Magazine, November/December, 1999, pp. 16-26.
- [51] S. Wang, F.C. Lee, D.Y. Chen, and W.G. Odendaal: *Effects of Parasitic Parameters on EMI Filter Performance*, IEEE Transactions on Power Electronics, Vol. 19, No. 3, May 2004, pp. 869-877.
- [52] S. Wang, F.C. Lee, W.G. Odendaal, and J.D. van Wyk: *Improvement of EMI Filter Performance with Parasitic Coupling Cancellation*, IEEE Transactions on Power Electronics, Vol. 20, No. 5, September 2005, pp. 1221-1228.
- [53] Teuvo Suntio, T. Tepsa, K. Kostov, and J. Kyrrä: *EMI Filter Design Issues in Switch-Mode Converter Applications*, PCIM 2004, Nürnberg, Germany, May 2004, pp. 830-835.
- [54] Teuvo Suntio, K. Kostov, T. Tepsa, and J. Kyrrä: *Using Input Invariance as a Method to Facilitate System Design in DPS Applications*, Journal of Circuits, Systems and Computers, Vol. 13, no. 4, August 2004, pp. 707-723.
- [55] Teuvo Suntio, T. Tepsa, K. Kostov, and J. Kyrrä: *EMI Filter Issues on Stability and Performance of Switched-Mode Converters*, EPE-PEMC 2004, Riga, Latvia, September, 2004, p 7.
- [56] Kurokawa, K., *Power Waves and the Scattering Matrix*, IEEE Transactions on Microwave Theory & Technology, March 1965, pp.194-202.
- [57] Roger B. Marks and Dylan F. Williams: *Comments on "Conversions Between S, Z, Y, h, ABCD, and T Parameters which are Valid for Complex Source and Load Impedances*, IEEE Transactions on Microwave Theory and Techniques, Vol. 43, No. 4, April 1995, pp. 914-915.
- [58] Michael Hiebel, *Fundamentals of Vector Network Analysis*, Rohde & Schwarz GmbH & Co., 2007, p. 419.

Appendices

A.1 Network Parameters

A.1.1 N-Port Network Parameters

A general n -port network is shown in Figure A.1. The $V_{s,i}$ and Z_i are respectively the Thévenin equivalent voltage source and impedance, seen from the i^{th} port. Assuming the network is linear, the port voltages and currents are the result of the simultaneous action of the sources. Using the superposition principle, the voltage and current at each port are the sum of the voltages and currents at that port, resulting from the excitations of each source, while the rest are set to zero.

Impedance z -parameters

The impedance z -parameters of an n -port network are the elements of the $n \times n$ impedance matrix \mathbf{Z} , i.e. the coefficient matrix in the following system of equations:

$$\begin{bmatrix} V_1 \\ V_2 \\ \vdots \\ V_n \end{bmatrix} = \begin{bmatrix} z_{11} & z_{12} & \cdots & z_{1n} \\ z_{21} & z_{22} & \cdots & z_{2n} \\ \vdots & \vdots & \ddots & \vdots \\ z_{n1} & z_{n2} & \cdots & z_{nn} \end{bmatrix} \begin{bmatrix} I_1 \\ I_2 \\ \vdots \\ I_n \end{bmatrix} \Leftrightarrow \mathbf{v} = \mathbf{Z}\mathbf{i} \quad (\text{A.1})$$

where \mathbf{v} is a vector of port voltages and its i^{th} element V_i , is the voltage at the i^{th} port. Similarly, \mathbf{i} is a vector of port currents and the i^{th} element of that vector is the current at the i^{th} port I_i .

The z -parameters are called open-circuit impedance parameters because the obvious way to measure them is to open-circuit all the ports except one, say the i^{th} port, and then measure the i^{th} current and all n voltages simultaneously. With these data, the i^{th} column

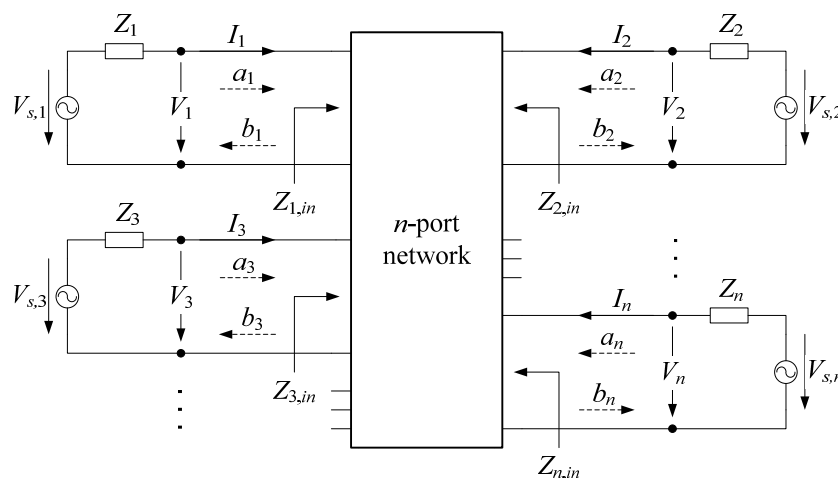


Figure A.1: An n -port network.

of \mathbf{Z} can be calculated. The procedure has to be repeated with all the remaining ports until all the elements of \mathbf{Z} are obtained. Clearly, this is a laborious measurement, but the greater disadvantage of z -parameters is their low measurement accuracy at higher frequencies. The open-circuited ports are no longer open-circuited when the voltage-measuring instrument is connected. In addition to the instrument's input impedance, there is also parasitic impedance at each port, which is unknown and affects the measured voltages. Even in the MHz range the ports parasitics can no longer be ignored, because they lead to larger and larger errors.

Admittance y -parameters

Of course, the linear system of equations (A.1) can be rewritten in such a way, that the dependent and independent variables change their roles. The result is an equivalent representation of the same system, where the coefficients are the so-called short-circuit admittance parameters, or simply y -parameters:

$$\begin{bmatrix} I_1 \\ I_2 \\ \vdots \\ I_n \end{bmatrix} = \begin{bmatrix} y_{11} & y_{12} & \cdots & y_{1n} \\ y_{21} & y_{22} & \cdots & y_{2n} \\ \vdots & \vdots & \ddots & \vdots \\ y_{n1} & y_{n2} & \cdots & y_{nn} \end{bmatrix} \begin{bmatrix} V_1 \\ V_2 \\ \vdots \\ V_n \end{bmatrix} \Leftrightarrow \mathbf{i} = \mathbf{Y}\mathbf{v} \quad (\text{A.2})$$

where \mathbf{Y} is the $n \times n$ admittance matrix, whose elements are the y -parameters. In this case, in order to measure the y -parameters, all the elements of \mathbf{v} except one must be set to zero. In other words, all the ports except one must be short-circuited. The disadvantages of z -parameters are valid for y -parameters as well, except that in this case the reason for low accuracy is the short-circuit impedance, which increases with the frequency. The \mathbf{Z} and \mathbf{Y} are square matrices of the same size, which are inverses of each other:

$$\mathbf{v} = \mathbf{Z}\mathbf{i} \Leftrightarrow \mathbf{Z}^{-1}\mathbf{v} = \mathbf{Z}^{-1}\mathbf{Z}\mathbf{i} = \mathbf{i} \Rightarrow \mathbf{Y} = \mathbf{Z}^{-1} \Leftrightarrow \mathbf{Z} = \mathbf{Y}^{-1} \quad (\text{A.3})$$

Therefore, knowing either one of these two sets of parameters would allow the calculation of the other set.

Scattering s -parameters

The s -parameters of an n -port network are the elements of the scattering matrix \mathbf{S} :

$$\begin{bmatrix} b_1 \\ b_2 \\ \vdots \\ b_n \end{bmatrix} = \begin{bmatrix} s_{11} & s_{12} & \cdots & s_{1n} \\ s_{21} & s_{22} & \cdots & s_{2n} \\ \vdots & \vdots & \ddots & \vdots \\ s_{n1} & s_{n2} & \cdots & s_{nn} \end{bmatrix} \begin{bmatrix} a_1 \\ a_2 \\ \vdots \\ a_n \end{bmatrix} \Leftrightarrow \mathbf{b} = \mathbf{S}\mathbf{a} \quad (\text{A.4})$$

Vectors \mathbf{a} and \mathbf{b} contain the incident and reflected power waves at all n ports. The i^{th} elements of these vectors, namely a_i and b_i , are respectively, the incident and reflected power waves from the i^{th} port. They are defined in [56] as:

$$a_i = \frac{V_i + Z_i I_i}{2\sqrt{|\text{Re}\{Z_i\}|}} \quad b_i = \frac{V_i - Z_i^* I_i}{2\sqrt{|\text{Re}\{Z_i\}|}} \quad (\text{A.5})$$

Where Z_i^* is the complex conjugate of Z_i .

Although the use of complex port impedances Z_i in (A.5) leads to an elegant theory, it is controversial, because it leads to a reflection coefficient:

$$\rho_i = \frac{Z_i - Z_0^*}{Z_i + Z_0} = \frac{Z_i/Z_0 - Z_0^*/Z_0}{Z_i/Z_0 + 1} \quad (\text{A.6})$$

Which is not uniquely determined if the reference impedance Z_0 is a complex one. This can lead to serious errors [57], because the basis for the Smith Chart is a reflection coefficient:

$$\rho_i = \frac{Z_i - Z_0}{Z_i + Z_0} = \frac{Z_i/Z_0 - 1}{Z_i/Z_0 + 1} \quad (\text{A.7})$$

which uniquely defines ρ_i in terms of Z_i and Z_0 . For this reason in practice Z_i and Z_0 are assumed to be positive and real. The power waves (A.5) then turn into normalized incident and reflected voltage waves:

$$a_i = \frac{V_i + R_0 I_i}{2\sqrt{R_0}} = \frac{V_{\text{wave incident at port } i}}{\sqrt{R_0}} \quad b_i = \frac{V_i - R_0 I_i}{2\sqrt{R_0}} = \frac{V_{\text{wave reflected from port } i}}{\sqrt{R_0}} \quad (\text{A.8})$$

The s -parameters are measured with VNA. Although scalar network analyzers do exist, they are out of consideration because of their significant disadvantages [58]. All the ports of a VNA have well-defined and equal port impedances, which is the measurement system's reference impedance, and therefore, in VNA measurement set-up $Z_i = Z_0 = R_0$ (usually 50Ω resistive). Furthermore, modern VNAs have sophisticated calibration, which minimizes the impact of the deviations in port impedances, connecting wires, and other factors causing systematic errors. As a result, s -parameter measurements are repeatable and accurate up to 40 GHz [58]. Thanks to their advantages they are the preferred set of network parameters nowadays. Whenever necessary, the other network parameters can be obtained by conversion from the measured s -parameters.

A.1.2 Two-Port Network Parameters

The special case of networks with two ports deserves special attention. In this case one of the two ports is assigned as an input port. The port voltage, current, and power waves at the input have the subscript 1. The second port, denoted by the subscript 2, is the output port. Figure A.2 shows a two-port network excited at its input by an electrical source, represented by its Thévenin equivalent voltage V_s with internal impedance Z_s .

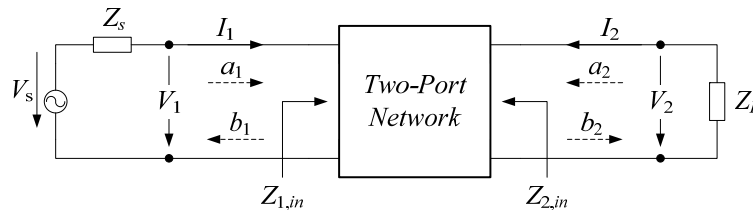


Figure A.2: A two-port network.

The output port is terminated by the load impedance Z_L .

In some textbooks, the direction of I_2 is reversed, but in the more general case of n -port networks, it makes sense to have a uniform definition for the port current as the one flowing into the port.

The two-port network parameters are defined as follows:

Hybrid h-parameters:

$$\begin{bmatrix} V_1 \\ I_2 \end{bmatrix} = \begin{bmatrix} h_{11} & h_{12} \\ h_{21} & h_{22} \end{bmatrix} \begin{bmatrix} I_1 \\ V_2 \end{bmatrix} \quad \mathbf{H} = \begin{bmatrix} h_{11} & h_{12} \\ h_{21} & h_{22} \end{bmatrix} \quad (\text{A.9})$$

Hybrid g-parameters:

$$\begin{bmatrix} I_1 \\ V_2 \end{bmatrix} = \begin{bmatrix} g_{11} & g_{12} \\ g_{21} & g_{22} \end{bmatrix} \begin{bmatrix} V_1 \\ I_2 \end{bmatrix} \quad \mathbf{G} = \begin{bmatrix} g_{11} & g_{12} \\ g_{21} & g_{22} \end{bmatrix} \quad (\text{A.10})$$

Chain c-parameters (also called cascade, transmission, or ABCD):

$$\begin{bmatrix} V_1 \\ I_1 \end{bmatrix} = \begin{bmatrix} c_{11} & c_{12} \\ c_{21} & c_{22} \end{bmatrix} \begin{bmatrix} V_2 \\ -I_2 \end{bmatrix} \quad \mathbf{C} = \begin{bmatrix} c_{11} & c_{12} \\ c_{21} & c_{22} \end{bmatrix} \quad (\text{A.11})$$

Admittance y-parameters:

$$\begin{bmatrix} I_1 \\ I_2 \end{bmatrix} = \begin{bmatrix} y_{11} & y_{12} \\ y_{21} & y_{22} \end{bmatrix} \begin{bmatrix} V_1 \\ V_2 \end{bmatrix} \quad \mathbf{Y} = \begin{bmatrix} y_{11} & y_{12} \\ y_{21} & y_{22} \end{bmatrix} \quad (\text{A.12})$$

Impedance z-parameters:

$$\begin{bmatrix} V_1 \\ V_2 \end{bmatrix} = \begin{bmatrix} z_{11} & z_{12} \\ z_{21} & z_{22} \end{bmatrix} \begin{bmatrix} I_1 \\ I_2 \end{bmatrix} \quad \mathbf{Z} = \begin{bmatrix} z_{11} & z_{12} \\ z_{21} & z_{22} \end{bmatrix} \quad (\text{A.13})$$

Scattering s-parameters:

$$\begin{bmatrix} b_1 \\ b_2 \end{bmatrix} = \begin{bmatrix} s_{11} & s_{12} \\ s_{21} & s_{22} \end{bmatrix} \begin{bmatrix} a_1 \\ a_2 \end{bmatrix} \quad \mathbf{S} = \begin{bmatrix} s_{11} & s_{12} \\ s_{21} & s_{22} \end{bmatrix} \quad (\text{A.14})$$

Scattering transmission t-parameters:

$$\begin{bmatrix} b_1 \\ a_1 \end{bmatrix} = \begin{bmatrix} t_{11} & t_{12} \\ t_{21} & t_{22} \end{bmatrix} \begin{bmatrix} a_2 \\ b_2 \end{bmatrix} \quad \mathbf{T} = \begin{bmatrix} t_{11} & t_{12} \\ t_{21} & t_{22} \end{bmatrix} \quad (\text{A.15})$$

The h - and g -parameters are called hybrid parameters, because of their different units. That should not be taken as a rule, because c -parameters also have different units, but

are not called hybrid. Instead, they have been called transmission, ABCD [44], or A -parameters [3]. The notation used in this thesis is consistent with the notations of the other network parameters and relates to the main advantage of c -parameters, which is that the c -parameters of cascade-connected (or chained) networks are obtained by matrix multiplication of their \mathbf{C} -matrices. The same is true for the t -parameters as well.

The z - and y -parameters are useful for series- and parallel-connected networks. The z -parameters of a network consisting of series-connected networks are obtained by adding the \mathbf{Z} -matrices of the individual networks. Similarly, the y -parameters of a network consisting of shunt-connected networks are the sum of the \mathbf{Y} -matrices of the individual networks.

A.2 The Input Impedances of Some Noise Separators

A.2.1 The Resistive Noise Separator in Figure 2.8a

The resistive noise separator in Figure 2.8a can be redrawn as in Figure A.3, which has the following mesh equations:

$$\begin{bmatrix} 25+25 & 25 \\ 25 & 25+25 \end{bmatrix} \begin{bmatrix} I_p \\ I_n \end{bmatrix} = \begin{bmatrix} V_p \\ V_n \end{bmatrix} \quad (\text{A.16})$$

From (A.16) the phase and neutral currents are:

$$I_p = \frac{\begin{vmatrix} V_p & 25 \\ V_n & 50 \end{vmatrix}}{\begin{vmatrix} 50 & 25 \\ 25 & 50 \end{vmatrix}} = \frac{50 \cdot V_p - 25 \cdot V_n}{50^2 - 25^2} = \frac{2 \cdot V_p - V_n}{75} \quad I_n = \frac{\begin{vmatrix} 50 & V_p \\ 25 & V_n \end{vmatrix}}{\begin{vmatrix} 50 & 25 \\ 25 & 50 \end{vmatrix}} = \frac{2 \cdot V_n - V_p}{75} \quad (\text{A.17})$$

Then the phase and neutral input impedances are:

$$Z_{in,p} = \frac{V_p}{I_p} = \frac{75 \cdot V_p}{2 \cdot V_p - V_n} \quad Z_{in,n} = \frac{V_n}{I_n} = \frac{75 \cdot V_n}{2 \cdot V_n - V_p} \quad (\text{A.18})$$

This proves (2.23) in Section 2.4.

A.2.2 The Transformer-Based Noise Separators in Figure 2.9a and c

In principle, the separators in Figure 2.9a and c are identical to the circuit shown in Figure A.4a. In Figure 2.9a resistor $R_1 = 82 \Omega$ and R_2 is the input impedance of the EMI measuring instrument, i.e. $R_2 = R_0 = 50 \Omega$. In Figure 2.9c resistor $R_1 = 150 \Omega$ and R_2 is the 150Ω resistor at the output in parallel with the input impedance of the measuring instrument, i.e. $R_2 = 50 \Omega \parallel 150 \Omega = 37.5 \Omega$. Assuming that both transformers have identical primary and secondary windings, the equivalent circuit of Figure A.4a is drawn in Figure A.4c.

The mesh equations for the circuit in Figure A.4c are:

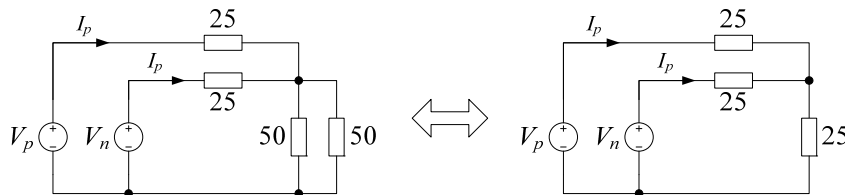


Figure A.3: Electrical circuit of the resistive noise separator in Figure 2.8a.

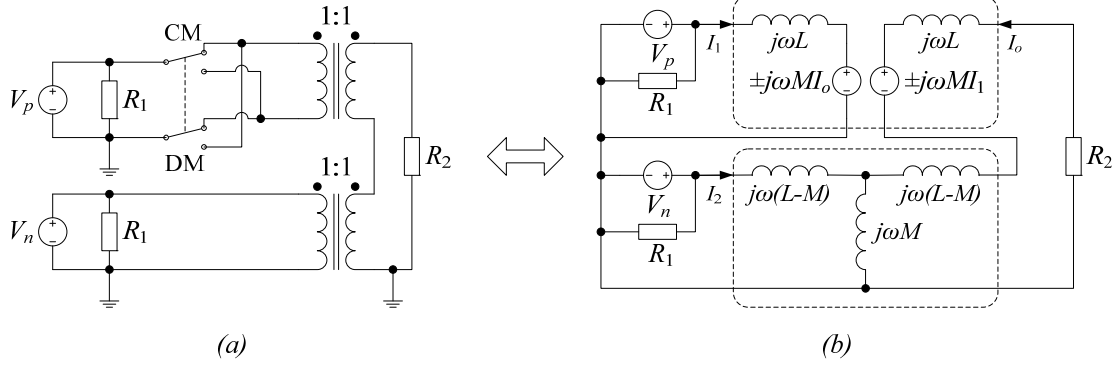


Figure A.4: Equivalent circuit of the noise separators in Figure 2.9a and c.

$$\begin{bmatrix} j\omega L & 0 & 0 \\ 0 & j\omega L & j\omega M \\ 0 & j\omega M & R_2 + j\omega 2L \end{bmatrix} \begin{bmatrix} I_1 \\ I_2 \\ I_o \end{bmatrix} = \begin{bmatrix} V_p \pm j\omega M I_o \\ V_n \\ \pm j\omega M I_1 \end{bmatrix} \quad (\text{A.19})$$

The \pm sign in (A.19) depends on the position of the DPDT switch. After the terms containing currents in the voltage vector have been moved to the left-hand side of the equations the system (A.19) becomes:

$$\begin{bmatrix} j\omega L & 0 & \pm j\omega M \\ 0 & j\omega L & j\omega M \\ \pm j\omega M & j\omega M & R_2 + j\omega 2L \end{bmatrix} \begin{bmatrix} I_1 \\ I_2 \\ I_o \end{bmatrix} = \begin{bmatrix} V_p \\ V_n \\ 0 \end{bmatrix} \quad (\text{A.20})$$

Assuming ideal transformers, i.e. $M = L$, from (A.20) the input phase current is:

$$I_1 = \frac{V_p \pm V_n}{R_2} - j \frac{V_p}{\omega L} \quad I_2 = \frac{V_n \pm V_p}{R_2} - j \frac{V_n}{\omega L} \quad (\text{A.21})$$

Then the phase and neutral input impedances are:

$$Z_{in,p} = R_1 \parallel \left(\frac{V_p}{I_1} \right) = R_1 \parallel \left[\frac{V_p \omega L R_2}{(V_p \pm V_n) \omega L - j V_p R_2} \right] \quad (\text{A.22})$$

$$Z_{in,n} = R_1 \parallel \left(\frac{V_n}{I_2} \right) = R_1 \parallel \left[\frac{V_n \omega L R_2}{(V_n \pm V_p) \omega L - j V_n R_2} \right] \quad (\text{A.23})$$

Equations (A.22) and (A.23) show that the input impedances of the circuits in Figure 2.9a and c are voltage-dependent.

A.3 Symmetrical T- and Π -Equivalents of the Diagonal Circuit

A.3.1 The Diagonal Circuit

The y -parameters of a two-port network are defined as:

$$y_{mn} = \left. \frac{I_m}{V_n} \right|_{V_m=0} \quad m, n = 1, 2 \quad (\text{A.24})$$

Then for the circuit in Figure A.5a the y -parameters are:

$$\begin{bmatrix} I_1 \\ I_2 \end{bmatrix} = \frac{1}{Z_{12} + Z_{21}} \begin{bmatrix} 1 & -1 \\ -1 & 1 \end{bmatrix} \begin{bmatrix} V_1 \\ V_2 \end{bmatrix} \quad (\text{A.25})$$

The y -parameters of the circuit in Figure A.5b are:

$$\begin{bmatrix} I_1 \\ I_2 \end{bmatrix} = \frac{1}{Z_{d1} + Z_{d2}} \begin{bmatrix} 1 & 1 \\ 1 & 1 \end{bmatrix} \begin{bmatrix} V_1 \\ V_2 \end{bmatrix} \quad (\text{A.26})$$

The diagonal circuit, shown in Figure A.5c, is formed by connecting in parallel the networks shown in Figure A.5a and b. Therefore the Y -matrix of the diagonal circuit is the sum of the Y -matrices of the paralleled networks:

$$\mathbf{Y}_d = \begin{bmatrix} \frac{1}{Z_{d1} + Z_{d2}} + \frac{1}{Z_{12} + Z_{21}} & \frac{1}{Z_{d1} + Z_{d2}} - \frac{1}{Z_{12} + Z_{21}} \\ \frac{1}{Z_{d1} + Z_{d2}} - \frac{1}{Z_{12} + Z_{21}} & \frac{1}{Z_{d1} + Z_{d2}} + \frac{1}{Z_{12} + Z_{21}} \end{bmatrix} \quad (\text{A.27})$$

In the case of symmetrical networks, i.e. when $Z_{12} = Z_{21} = Z_t$ and $Z_{d1} = Z_{d2} = Z_d$:

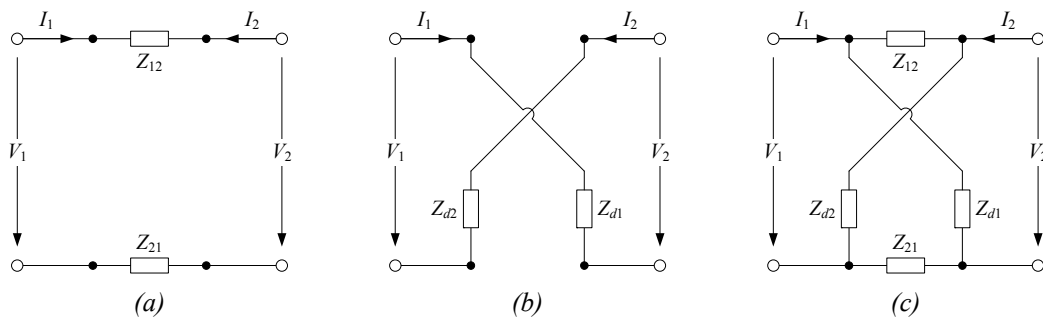


Figure A.5: The diagonal circuit:

The diagonal circuit in c) is the parallel connection of the networks in a) and b).

$$\mathbf{Y}_d = \frac{1}{2} \begin{bmatrix} \frac{1}{Z_d} + \frac{1}{Z_t} & \frac{1}{Z_d} - \frac{1}{Z_t} \\ \frac{1}{Z_d} - \frac{1}{Z_t} & \frac{1}{Z_d} + \frac{1}{Z_t} \end{bmatrix} = \frac{1}{2} \begin{bmatrix} Y_d + Y_t & Y_d - Y_t \\ Y_d - Y_t & Y_d + Y_t \end{bmatrix} \quad (\text{A.28})$$

A.3.2 The T-circuit

When the mesh method is applied to the T-circuit in Figure A.6a:

$$\begin{bmatrix} V_1 \\ V_2 \end{bmatrix} = \begin{bmatrix} Z_{s1} + Z_p + Z_{s3} & Z_p \\ Z_p & Z_{s2} + Z_p + Z_{s4} \end{bmatrix} \begin{bmatrix} I_1 \\ I_2 \end{bmatrix} = \mathbf{Z}_T \begin{bmatrix} I_1 \\ I_2 \end{bmatrix} \quad (\text{A.29})$$

where \mathbf{Z}_T is the \mathbf{Z} -matrix of the T-circuit. Its y -parameters are:

$$\mathbf{Y}_T = \mathbf{Z}_T^{-1} = \frac{\begin{bmatrix} Z_{s2} + Z_p + Z_{s4} & -Z_p \\ -Z_p & Z_{s1} + Z_p + Z_{s3} \end{bmatrix}}{(Z_{s1} + Z_p + Z_{s3})(Z_{s2} + Z_p + Z_{s4}) - Z_p^2} \quad (\text{A.30})$$

In the special case of a symmetrical T-circuit (Figure A.6b), i.e. when impedances $Z_{s1} = Z_{s2} = Z_{s3} = Z_{s4} = Z_s$, then (A.30) becomes:

$$\mathbf{Y}_T = \frac{1}{4Z_s(Z_s + Z_p)} \begin{bmatrix} 2Z_s + Z_p & -Z_p \\ -Z_p & 2Z_s + Z_p \end{bmatrix} \quad (\text{A.31})$$

A.3.3 Symmetrical T-equivalent of the Symmetrical Diagonal Circuit

When the y -parameters in (A.28) and (A.31) are equal, then the symmetrical T-circuit is equivalent to the symmetrical diagonal circuit. Obviously the condition for that is:

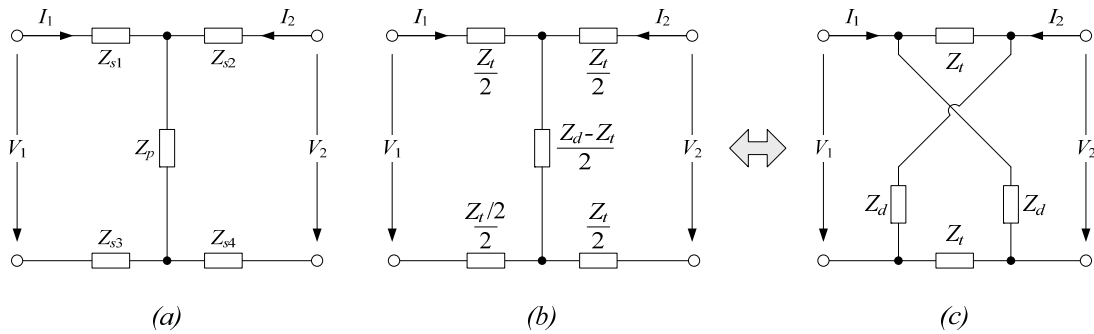


Figure A.6: T-equivalent of a symmetrical diagonal circuit:

a) T-circuit; b) symmetrical T-circuit that is equivalent to c) the symmetrical diagonal circuit.

$$\begin{cases} \frac{1}{Z_d} + \frac{1}{Z_t} = \frac{2Z_s + Z_p}{2Z_s(Z_s + Z_p)} \\ \frac{1}{Z_d} - \frac{1}{Z_t} = \frac{-Z_p}{2Z_s(Z_s + Z_p)} \end{cases} \Leftrightarrow \begin{cases} Z_p = \frac{Z_d - Z_t}{2} \\ Z_s = \frac{Z_t}{2} \end{cases} \quad (\text{A.32})$$

which is depicted by the equivalent circuits in Figure A.6b and c.

A.3.4 The Π -circuit

The symmetrical π -circuit in Figure A.7a can be viewed as a parallel connection of the networks in Figure A.5a and Figure A.7b. The latter has the following y -parameters:

$$\begin{bmatrix} I_1 \\ I_2 \end{bmatrix} = \begin{bmatrix} Y_{11} & 0 \\ 0 & Y_{22} \end{bmatrix} \begin{bmatrix} V_1 \\ V_2 \end{bmatrix} \quad (\text{A.33})$$

Then the y -parameters of the π -circuit are obtained by adding the \mathbf{Y} -matrices in (A.25) and (A.33) for I_a and I_b gives the y -parameters for the π -circuit:

$$\mathbf{Y}_\pi = \begin{bmatrix} Y_{11} + \frac{1}{Z_{12} + Z_{21}} & -\frac{1}{Z_{12} + Z_{21}} \\ -\frac{1}{Z_{12} + Z_{21}} & Y_{22} + \frac{1}{Z_{12} + Z_{21}} \end{bmatrix} \quad (\text{A.34})$$

In the special case of a symmetrical π -circuit, i.e. when admittances $Y_{11} = Y_{22} = Y_{\pi 1}$ and impedances $Z_{12} = Z_{21} = Z_{\pi 2} = 1/Y_{\pi 2}$, then (A.34) becomes:

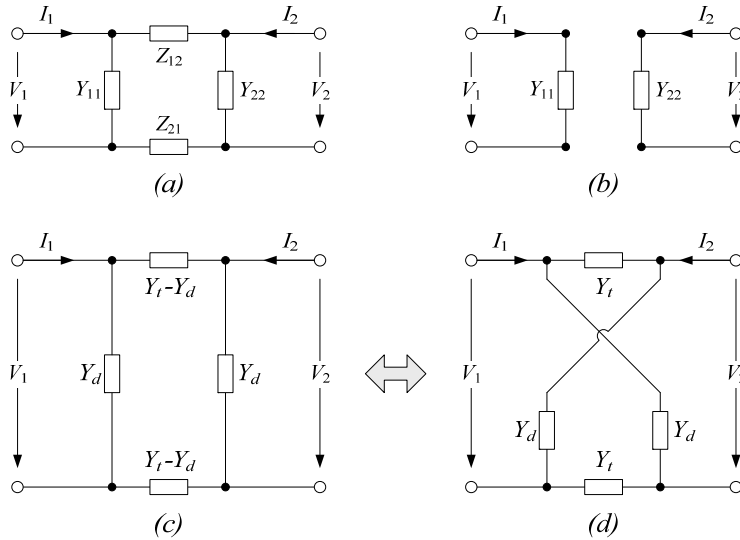


Figure A.7: Π -equivalent of a symmetrical diagonal circuit:

- a) a π -circuit can be seen as a parallel connection of circuit b) and the circuit in **Figure A.5a**;
- c) symmetrical π -circuit, equivalent to d) the symmetrical diagonal circuit.

$$\mathbf{Y}_\pi = \frac{1}{2} \begin{bmatrix} 2Y_{\pi 1} + Y_{\pi 2} & -Y_{\pi 2} \\ -Y_{\pi 2} & 2Y_{\pi 1} + Y_{\pi 2} \end{bmatrix} \quad (\text{A.35})$$

A.3.5 Symmetrical Π -equivalent of the Symmetrical Diagonal Circuit

When the y -parameters in (A.28) and (A.35) are equal, then the symmetrical π -circuit is equivalent to the symmetrical diagonal circuit:

$$\begin{cases} Y_d + Y_t = 2Y_{\pi 1} + Y_{\pi 2} \\ Y_d - Y_t = -Y_{\pi 2} \end{cases} \Leftrightarrow \begin{cases} Y_{\pi 1} = Y_d \\ Y_{\pi 2} = Y_t - Y_d \end{cases} \quad (\text{A.36})$$

which is depicted by the equivalent circuits in Figure A.7*c* and *d*.

Note that, as expected, the general diagonal, T-, and π -circuits, are reciprocal, i.e. $y_{12} = y_{21}$. In addition, their symmetrical versions also have $y_{11} = y_{22}$.

A.4 CM and DM Inductance of Coupled Inductors

Two coupled inductors, whether they are DM or CM chokes, can be viewed as four-port network. With port voltages and currents as in Figure A.8, the voltages across each of the two windings are as follows:

$$\begin{aligned} V_1 - V_3 &= L_1 \frac{di_1}{dt} \pm M \frac{di_2}{dt} \\ V_2 - V_4 &= \pm M \frac{di_1}{dt} + L_2 \frac{di_2}{dt} \end{aligned} \quad (\text{A.37})$$

In (A.37) and in the following equations, the upper sign in front of M applies to CM chokes and the lower one applies to coupled DM inductors. Assume that the input ports are denoted by subscripts 1 and 2, and the outputs are 3 and 4. From (A.37) and using the definitions (2.8) and (2.11), the CM and DM voltages at the input and output are:

$$\begin{aligned} V_{cm,i} &= \frac{V_1 + V_2}{2} = \frac{L_1 \pm M}{2} \frac{di_1}{dt} + \frac{L_2 \pm M}{2} \frac{di_2}{dt} + V_{cm,o} \\ V_{dm,i} &= V_1 - V_2 = (L_1 \mp M) \frac{di_1}{dt} - (L_2 \mp M) \frac{di_2}{dt} + V_{dm,o} \end{aligned} \quad (\text{A.38})$$

Assuming identical inductances on both paths, the following condition is fulfilled:

$$L_1 = L_2 = L \quad (\text{A.39})$$

where L is the inductance per path. Then (A.38) becomes:

$$\begin{aligned} V_{cm,i} &= \frac{L \pm M}{2} \frac{d(i_1 + i_2)}{dt} + V_{cm,o} \\ V_{dm,i} &= (L \mp M) \frac{d(i_1 - i_2)}{dt} + V_{dm,o} \end{aligned} \quad (\text{A.40})$$

Using the definitions (2.6) and (2.10) for CM and DM current, (A.40) becomes:

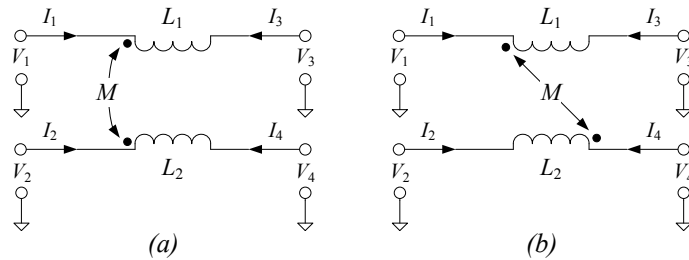


Figure A.8: a) CM choke; b) coupled DM inductors.

$$\begin{aligned}
i_{cm} &= i_1 + i_2 & V_{cm,i} &= \frac{L \pm M}{2} \frac{di_{cm}}{dt} + V_{cm,o} = L_{cm} \frac{di_{cm}}{dt} + V_{cm,o} \\
i_{dm} &= \frac{i_1 - i_2}{2} & \Rightarrow & & V_{dm,i} &= 2(L \mp M) \frac{di_{dm}}{dt} + V_{dm,o} = L_{dm} \frac{di_{dm}}{dt} + V_{dm,o}
\end{aligned} \tag{A.41}$$

Therefore the equivalent CM and DM inductances for a CM choke are:

$$L_{cm} = \frac{L + M}{2} \quad \text{and} \quad L_{dm} = 2(L - M) \tag{A.42}$$

And the equivalent CM and DM inductances for coupled DM inductors:

$$L_{cm} = \frac{L - M}{2} \quad \text{and} \quad L_{dm} = 2(L + M) \tag{A.43}$$

The coupling coefficient between the winding is defined as:

$$k = \frac{M}{\sqrt{L_1 L_2}} \quad \text{and} \quad 0 \leq |k| \leq 1 \tag{A.44}$$

Although the focus of this section is on coupled inductors, it is interesting to note that from (A.43), for decoupled inductors, i.e. when $k = 0 \Leftrightarrow M = 0$, the equivalent CM and DM inductances are:

$$L_{cm} = \frac{L}{2} \quad \text{and} \quad L_{dm} = 2L \tag{A.45}$$

which is the case shown in Figure 3.1 and in most of the literature.

In the case of coupled DM inductors with $k = 1$, i.e. when $L_1 = L_2 = L = M$:

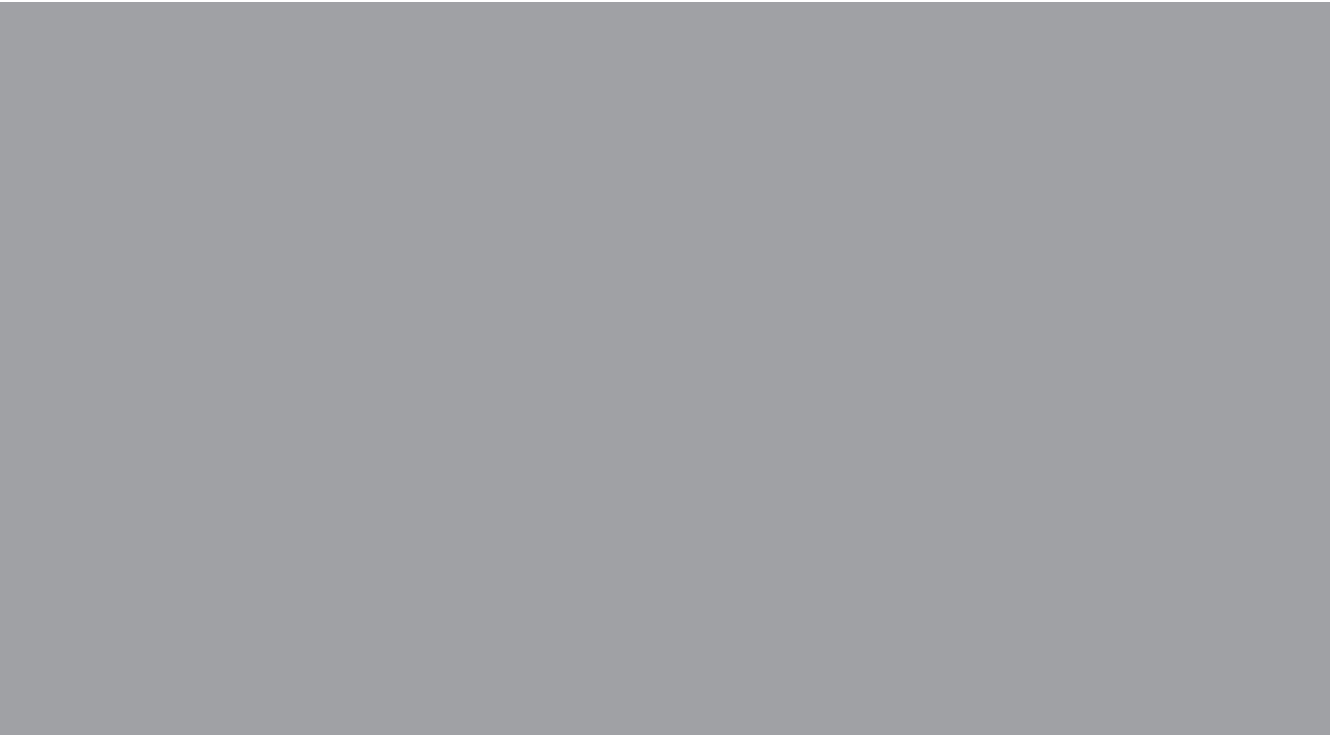
$$L_{cm} = 0 \quad \text{and} \quad L_{dm} = 4L \tag{A.46}$$

Therefore, the CM equivalent circuit in Figure 3.1b is not valid for coupled DM inductors, because their CM inductance is not half of the inductance per path, but zero. In practice, coupled DM inductors would provide some CM attenuation because in reality $k < 1$.

For CM chokes, if $k = 1$, i.e. when $L_1 = L_2 = L = M$:

$$L_{cm} = L \quad \text{and} \quad L_{dm} = 0 \tag{A.47}$$

In reality, because $k < 1$, i.e. there is always some leakage flux and there is always some leakage inductance L_{dm} in accordance with (A.42).



ISBN 978-952-248-186-3
ISBN 978-952-248-187-0 (PDF)
ISSN 1795-2239
ISSN 1795-4584 (PDF)